

***Supplementary information for
N,N'-octyl biphenothiazine and dibenzothiophene dioxide-based
soluble porous organic polymer for biphasic photocatalytic
hydrogen evolution***

Madhurima Sarkar and Abhijit Patra*

Department of Chemistry, Indian Institute of Science Education and Research Bhopal,
Bhopal Bypass Road, Bhauri, Bhopal 462066, Madhya Pradesh, India

Email: abhijit@iiserb.ac.in

Sr. no	Contents	Page no.
I	Materials and methods	S2-S4
a	Chemicals	S2
b	Instrumentation	S2-S4
II	Design strategy	S5
III	Synthesis and characterization	S6-S17
a	Synthesis and characterization of the monomers	S6-S10
b	Synthesis of the soluble porous organic polymer (PzDBS), soluble linear organic polymer (PzBDS-L) and insoluble porous organic polymer (PzDBS-C)	S11-S12
c	Characterization of PzDBS	S13-S15
d	Characterization of PzDBS-L	S16-S17
IV	Microscopic characterizations of PzDBS-L (FESEM, HRTEM)	S18
V	Surface area analysis of PzDBS-L	S19
VI	Characterization of PzDBS-C	S19
VII	Spectroscopic study of PzDBS and PzDBS-L	S20-S21
VIII	Electrochemical study of PzDBS and PzDBS-L	S21-S22
IX	Calibration curve for the estimation of evolved hydrogen	S23
X	Optimization of the photocatalytic reaction conditions	S24-S25
XI	Photocatalytic hydrogen evolution: biphasic vs. heterogeneous	S26-S27
XII	Contact angle measurement of PzDBS and PzDBS-L	S27
XIII	Absorption, FESEM, and FTIR of the recycled catalyst (PzDBS)	S27-S28
XIV	ICP-OES analysis	S28
XV	Steady-state emission and lifetime analysis	S28-S29
XVI	Computational investigation	S30
XVII	¹ H NMR, ¹³ C NMR, and Mass spectra	S31-S41
XVIII	References	S42

I. Materials and methods

(a) Chemicals:

Chemicals were received in adequate purity and used directly unless otherwise specified. Phenothiazine (98%), 1,8-dibromooctane (98%), 1,6-dibromohexane (96%), potassium *tert*-butoxide (98%), dibenzothiophene dioxide (97%), 1-bromooctane (99%), *N*-bromosuccinimide (99%), bis(pinacolato)diboron (99%), potassium acetate (99%), 1[1,1'-Bis(diphenylphosphino)ferrocene]dichloropalladium(II), 1,1'-ferrocenediyl-bis(diphenylphosphine) (99%), tetrakis(triphenylphosphine)palladium(0) (99%), tetrabutylammonium bromide (98%), tetrabutylammonium hexafluorophosphate (99%), sodium sulphate (99%), magnesium sulphate (99%), nafion, triethylamine, triethanolamine, ascorbic acid, (99.85%), dimethyl sulfoxide (99%) were purchased from Sigma-Aldrich. Sulphuric acid (concentrated), chloroform, and 1,4-dioxane were obtained from Merck. Tetrahydrofuran (99%), dichloromethane, and ethanol (99.8%) were obtained from Spectrochem.

(b) Instrumentation:

^1H and ^{13}C -NMR spectra were recorded in Bruker Avance III NMR spectrometer. The high-resolution mass spectrometry (HRMS) data was obtained through Bruker MicrOTOF-Q-II mass spectrometer. UV-Vis absorption spectra were recorded in Cary 100 absorption spectrophotometer. Perkin-Elmer Model UATR Spectrum instrument was used for FTIR measurements. Data were recorded via signal-averaged values of 10 scans with 4 cm^{-1} resolutions at room temperature. Jobin Yvon Horiba Model Fluorolog-3-21 was used to record the steady-state fluorescence spectra. A time-correlated single-photon counting (TCSPC) spectrometer (Delta Flex-01-DD) was used for recording the time-resolved fluorescence spectra. A Delta diode laser of 405 nm was used as the excitation source. IBH DAS6 (version 6.8) software was used for decay curve analysis, and the quality of the fitting was assessed by χ^2 . The thermal stability was checked using a Perkin Elmer TGA-6000 instrument under a nitrogen environment (heating rate: $10\text{ }^\circ\text{C min}^{-1}$, temperature range: $30\text{-}800\text{ }^\circ\text{C}$). The Carl Zeiss (Ultraplus) field emission scanning electron microscope with accelerating voltage of 5 kV and 20 kV was used to examine the morphology of the polymer. The amorphous nature of the polymer was checked through high-resolution transmission electron microscopy (HRTEM) using FEI TALOS 200S instrument at a working voltage of 200 kV. The Quantachrome Autosorb, QUA211011 equipment was used for the measurement of gas adsorption. Before analysis, the sample was vacuum-degassed at $100\text{ }^\circ\text{C}$ for 24 h. ASiQwin software was used to analyze the isotherms.

Gel permeation chromatography (GPC):

GPC (Polymer Laboratories) was used for the estimation of the molecular weight of the soluble polymer. The calibration was carried out with polystyrene standard. We utilized PLGel mixed D and mixed C columns, and the flow rate of tetrahydrofuran (THF) was fixed at 1 mL min⁻¹ at 40 °C. The refractive index of the eluent: $n(c) = n_s + \frac{\delta n}{\delta c}c + \dots$, where c represents the concentration of the eluting polymer in g mL⁻¹, whereas n_s and $\frac{\delta n}{\delta c}$ represent the solvent's refractive index and its increment, respectively. The refractive index (n_s) and ($\frac{\delta n}{\delta c}$) of 1.404 for THF and 0.185 mL g⁻¹ for the polystyrene standards, respectively, were considered.

Cyclic voltammetry:

BioLogic SP300 potentiostat (BioLogic, France) was used for the cyclic voltammetry measurements in a three-electrode electrochemical cell in dichloromethane (Glassy carbon: working electrode, WE; platinum: counter electrode, CE; Ag/AgCl: reference electrode, RE). 0.1 M tetrabutylammonium hexafluorophosphate (TBAP) was used as a supporting electrolyte.

Mott–Schottky analysis:

The energy band position of the PzDBS polymer was calculated by the Mott Schottky (MS) analysis (at 2500 Hz, from 0 V to +1.0 V) in the deoxygenated aqueous solution of 0.5 M Na₂SO₄ in a three-electrode system using polymer electrochemical ink coated indium tin oxide (ITO) as a working electrode. The electrochemical ink was prepared by dispersing PzDBS (2.0 mg) for 30 minutes in 50 μL nafion solution and 450 μL ethanol. 42 mg of nafion was dissolved in 2 mL ethanol to prepare the nafion solution. The well-dispersed ink was drop casted over the ITO electrode and kept for drying overnight under ambient conditions. The valence band potential for PzDBS was estimated based on flat band potentials.

Photoelectrochemical study:

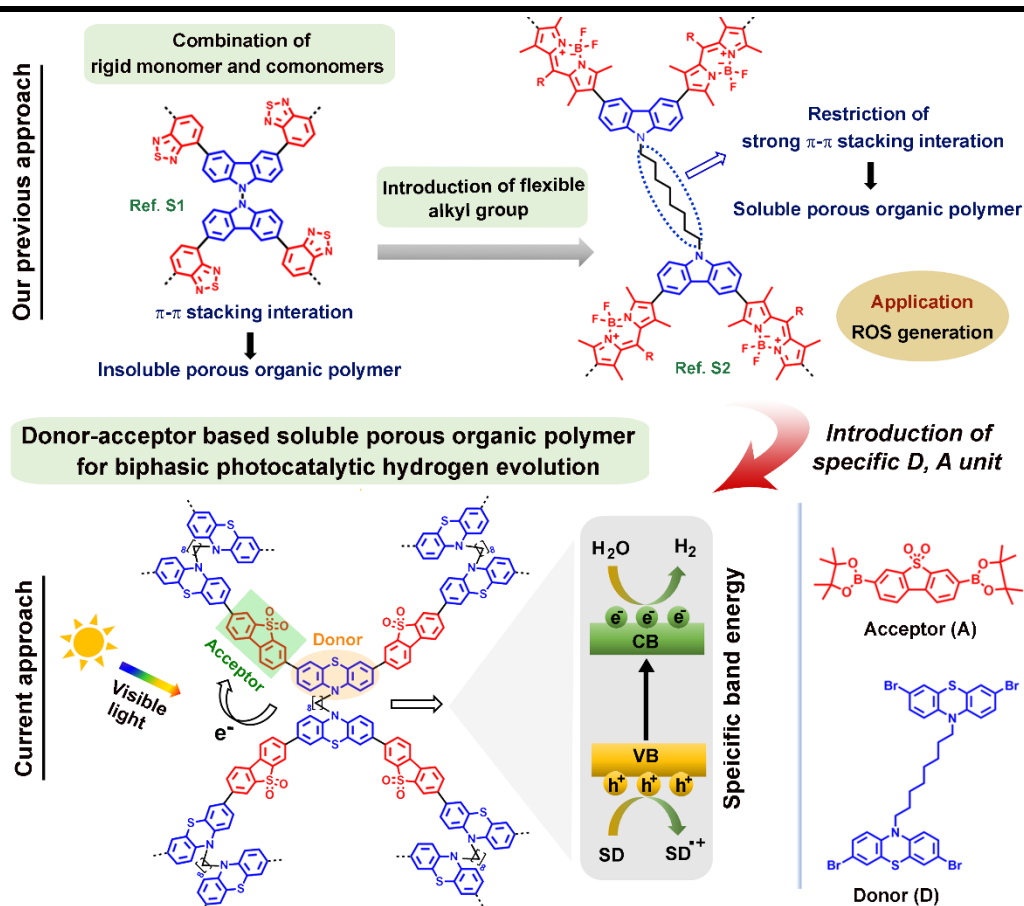
Electrochemical impedance analysis was carried out in the deoxygenated aqueous solution of 0.5 M Na₂SO₄ in a three-electrode system using polymer electrochemical ink coated indium tin oxide (ITO) as a working electrode. The electrochemical ink was prepared the same way as discussed in the Mott–Schottky analysis. The electrochemical impedance was measured between 100 kHz and 10 MHz at 0 V vs. Ag/AgCl under the dark and white light (50 Watt) irradiation.

The electrode was fabricated for the photocurrent measurements following the similar fabrication methodology of the Mott-Schottky analysis. Here, the photocurrent study was performed for the polymer over multiple cycles upon repeated light "ON-OFF" for 20 s at 0 V vs. Ag/AgCl.

General procedure for photocatalytic hydrogen evolution in aqueous-organic biphasic medium:

Photocatalytic hydrogen (H₂) evolution experiments were performed in a 30 mL borosilicate Schlenk tube containing a magnetic stir bar sealed with a septum. 2 mg of catalyst (either PzDBS or PzDBS-L) was taken into the Schlenk tube. Dichloromethane (DCM), water, and triethylamine (TEA), 3 mL each, were added to the tube. Then, the nitrogen purging was carried out with the reaction mixture for 20 minutes, followed by nitrogen/ vacuum cycles three times to remove any traces of dissolved H₂ gas, which was confirmed by GC investigation prior to the photocatalysis reaction. Upon irradiation with a 300 W Xe lamp (Lelesil innovative system) for the requisite time, the headspace gases were collected by a Hamilton air-tight syringe and were analyzed using a gas chromatograph equipped with a thermal conductivity detector (Shimadzu GC TCD 2030). Photocatalysis under visible light irradiation was carried out using a mercury-vapor lamp (390-650 nm).

II. Design strategy

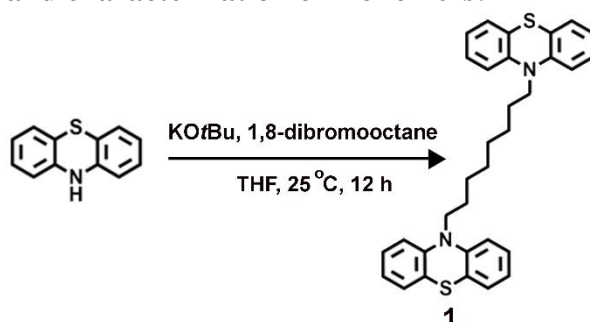


Scheme S1 Schematic diagram of the previous design strategies for the synthesis of insoluble porous organic polymer using carbazole and benzothiadiazole and soluble porous organic polymer using alkylated carbazole and boron dipyrromethene in order to produce reactive oxygen species (ROS). Schematic illustration demonstrating the current donor-acceptor-based design strategy for the synthesis of soluble porous organic polymer using alkylated phenothiazine and dibenzothiophene dioxide for biphasic photocatalytic hydrogen evolution; SD: sacrificial electron donor, VB: valence band, CB: conduction band.

The restriction of the high degree of crosslinking and fine-tuning of the non-covalent interactions in the network polymers through proper choice of monomers are the key to designing the soluble porous organic polymer. The presence of *N,N'*-bicarbazole linkage in the polymer causes strong π - π stacking.¹ While the introduction of the alkyl group between the two carbazole units induces solubility, reducing the π stacking while retaining the porosity in the polymer.² Bicarbazole-based soluble and insoluble polymers were explored earlier to produce reactive oxygen species (ROS). However, the design and development of a soluble porous organic polymer with specific band energy for targeted photocatalysis are rare. So, here we have designed and developed a donor-acceptor-based soluble porous organic polymer using alkylated phenothiazine and dibenzothiophene dioxide and have explored for the unique aqueous-organic biphasic photocatalytic hydrogen evolution.

III. Synthesis and characterization

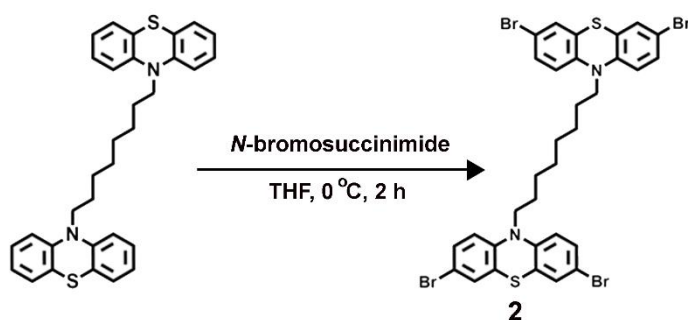
(a) Synthesis and characterization of monomers:



Scheme S2 Schematic illustration of the synthetic pathway of 1,8-di(10H-phenothiazine-10-yl)octane (1).

Synthesis of 1,8-di(10H-phenothiazine-10-yl)octane (1): 1,8-Di(10H-phenothiazine-10-yl)octane was synthesized following a reported method with certain modifications (Scheme S2).³ Phenothiazine (2.0 mmol) and potassium *tert*-butoxide (3.2 mmol) were taken in a Schlenk tube. N₂/vacuum cycle was carried out three times. After that, dry THF (10 mL) was added. The mixture was stirred at 25 °C for 12 h after the addition of 1,8-dibromooctane (0.8 mmol) and quenched by adding water after completion of the reaction. The organic phase was extracted with dichloromethane, followed by drying over anhydrous sodium sulphate (Na₂SO₄). Silica gel column chromatography was performed to purify the residue after the solvent evaporation using hexane/dichloromethane (V/V, 8/2) as the eluent (85% yield, Scheme S2).

¹H NMR (500 MHz, CDCl₃, δ): 7.16 (s, 8H), 6.94 (s, 8H), 3.83 (s, 4H), 1.76 (s, 4H), 1.35 (m, 8H). **¹³C NMR (126 MHz, CDCl₃, δ):** 145.29, 127.44, 127.18, 124.96, 122.36, 115.46, 47.36, 29.05, 26.73. **HRMS (ESI):** calculated for C₃₂H₃₂N₂S₂ is 508.74 and found 508.2017 [M⁺].



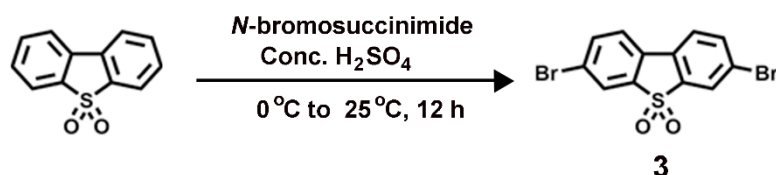
Scheme S3 Schematic illustration of the synthetic pathway of 1,8-bis(3,7-dibromo-10H-phenothiazine-10-yl)octane (2).

Synthesis of 1,8-bis(3,7-dibromo-10H-phenothiazine-10-yl)octane (BDPzO, 2): 1,8-Bis(3,7-dibromo-10H-phenothiazine-10-yl)octane was synthesized following a reported method with slight modification (Scheme S3).⁴ **1** (0.35 mmol) and *N*-bromo succinimide (NBS, 1.94 mmol) were taken in a Schlenk tube. N₂/vacuum cycle was carried out three times. After that, dry THF

(10 mL) was added and stirred at 0 °C for 2 h. After completion of the reaction, water was added to quench it. Dichloromethane was added to extract the organic phase, followed by drying over anhydrous sodium sulphate (Na₂SO₄). Silica gel column chromatography was carried out to purify the residue after the solvent evaporation using hexane/dichloromethane (V/V, 9/1) as the eluent (44% yield, Scheme S3).

¹H NMR (500 MHz, CDCl₃, δ): 7.23 (m, 8H), 6.66 (s, 4H), 3.73 (m, 4H), 1.69 (m, 4H), 1.27 (m, 8H). **¹³C NMR (126 MHz, CDCl₃, δ):** 144.19, 130.27, 129.90, 126.74, 116.85, 114.94, 47.60, 29.08, 26.67. **HRMS (ESI):** calculated for C₃₂H₂₈Br₄N₂S₂ is 824.33 and found 824.8450 [M⁺].

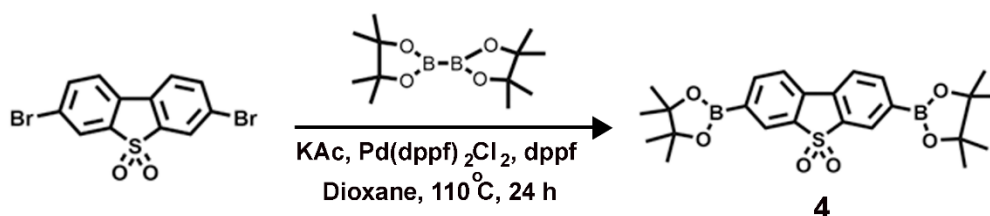
3,7-Dibromodibenzothiophene dioxide (**3**) and 3,7-bis(4,4,5,5-tetramethyl-1,3,2-dioxaborolan-2-yl) dibenzothiophene dioxide (**4**) were synthesized following a reported method with certain modification (Scheme S4 and S5).⁵



Scheme S4 Schematic illustration of the synthetic pathway of 3,7-dibromodibenzothiophene dioxide (**3**).

Synthesis of 3,7-dibromodibenzothiophene dioxide (3): NBS (6.39 mmol) was added at 0 °C to a solution of dibenzothiophene dioxide (2.13 mmol) in concentrated H₂SO₄ (30 mL). The mixture was poured into cold water following the reaction for 10 h at 25 °C. The crude solid was filtrated and repeatedly washed with water, followed by recrystallization in chlorobenzene to get a white solid (52% yield, Scheme S4).

¹H NMR (500 MHz, CDCl₃, δ): 7.93 (d, *J* = 1.6 Hz, 2H), 7.77 (m, 2H), 7.63 (d, *J* = 8.2 Hz, 2H). **¹³C NMR (126 MHz, CDCl₃, δ):** 139.06, 137.29, 129.75, 125.74, 124.75, 123.06. **HRMS (ESI):** calculated for C₁₂H₆Br₂O₂S is 374.05 and found 374.8507 [M⁺].

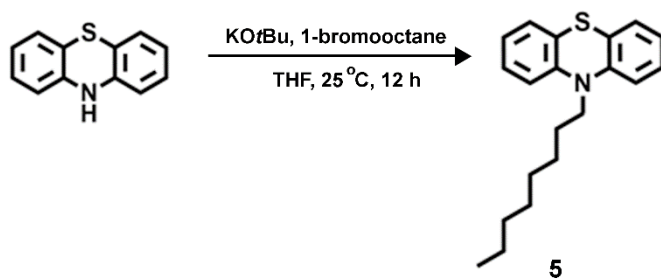


Scheme S5 Schematic illustration of the synthetic pathway of 3,7-bis(4,4,5,5-tetramethyl-1,3,2-dioxaborolan-2-yl) dibenzothiophene dioxide (**4**); KAc: potassium acetate, dppf: 1,1'-bis(diphenylphosphino)ferrocene.

Synthesis of 3,7-bis(4,4,5,5-tetramethyl-1,3,2-dioxaborolan-2-yl) dibenzothiophene dioxide (TDDBS, 4): 3,7-Dibromodibenzothiophene dioxide (0.4 mmol), bis(pinacolato)diboron (1.2

mmol) and potassium acetate (2 mmol) were added into a Schlenk tube. Nitrogen-vacuum cycles were carried out three times. After that, Pd(dppf)₂Cl₂ (4 mol %) and dppf (4 mol %) were added. Then, dry 1,4-dioxane (20 mL) was added and stirred at 110 °C for 24 h. After completion of the reaction, water was added to quench it. The organic phase was extracted with dichloromethane, followed by drying over anhydrous sodium sulphate (Na₂SO₄). Silica gel column chromatography was carried out to purify the residue after the solvent evaporation using hexane/dichloromethane (V/V, 5/5) as the eluent (60% yield, Scheme S5).

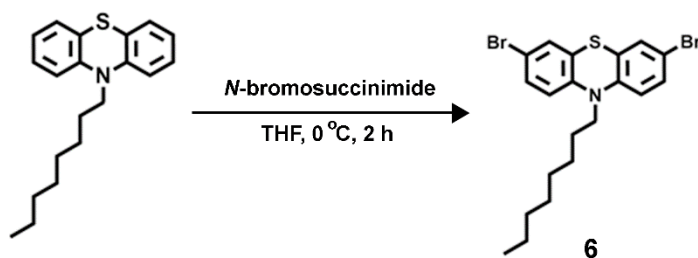
¹H NMR (500 MHz, CDCl₃, δ): δ 8.28 (s, 2H), 8.05 (d, *J* = 7.7 Hz, 2H), 7.80 (d, *J* = 7.7 Hz, 2H), 1.37 - 1.35 (m, 24H). **¹³C NMR (126 MHz, CDCl₃, δ):** 140.17, 137.66, 133.90, 128.54, 121.19, 84.71, 25.01. **HRMS (ESI):** calculated for C₂₄H₃₀B₂O₆S is 468.18 and found 469.2039 [M+H⁺].



Scheme S6 Schematic illustration of the synthetic pathway of 10-octyl-10H-phenothiazine (**5**).

Synthesis of 10-octyl-10H-phenothiazine (5): 10-Octyl-10H-phenothiazine was synthesized following a reported method with certain modifications (Scheme S6).³ Phenothiazine (5.0 mmol) and potassium *tert*-butoxide (6 mmol) were taken in a Schlenk tube. N₂/vacuum cycle was carried out three times. After that, dry THF (10 mL) was added. The mixture was stirred at 25 °C for 12 h after the addition of 1-dibromooctane (5 mmol) and quenched by adding water after completion of the reaction. The organic phase was extracted with dichloromethane, followed by drying over anhydrous sodium sulphate (Na₂SO₄). Silica gel column chromatography was performed to purify the residue after the solvent evaporation using hexane/dichloromethane (V/V, 8/2) as the eluent (78% yield, Scheme S6).

¹H NMR (500 MHz, CDCl₃, δ): 7.16 (m, 4H), 6.91 (m, 4H), 3.86 (m, 2H), 1.82 (m, 2H), 1.38 (m, 12H), 0.89 (m, 3H). **¹³C NMR (126 MHz, CDCl₃, δ):** 145.46, 127.54, 127.28, 125.02, 122.42, 115.50, 47.55, 31.88, 29.34, 27.11, 22.76, 14.23. **HRMS (ESI):** calculated for C₂₀H₂₅NS is 311.49 and found 312.1780 [M+H⁺].

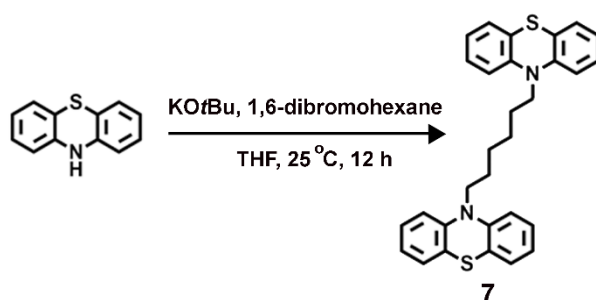


Scheme S7 Schematic illustration of the synthetic pathway of 3,7-dibromo-10-octyl-10H-phenothiazine (**6**).

Synthesis of 3,7-dibromo-10-octyl-10H-phenothiazine (6**):**

3,7-Dibromo-10-octyl-10H-phenothiazine was synthesized following a reported method with slight modification (Scheme S7).⁴ **5** (1.09 mmol) and *N*-bromo succinimide (NBS, 2.2 mmol) were taken in a Schlenk tube. N₂/vacuum cycle was carried out three times. After that, dry THF (10 mL) was added and stirred at 0 °C for 2 h. After completion of the reaction, water was added to quench it. Dichloromethane was added to extract the organic phase, followed by drying over anhydrous sodium sulphate (Na₂SO₄). Silica gel column chromatography was carried out to purify the residue after the solvent evaporation using hexane/dichloromethane (V/V, 9/1) as the eluent (50% yield, Scheme S7).

¹H NMR (500 MHz, CDCl₃, δ): 7.23 (m, 4H), 6.68 (m, 2H), 3.75 (m, 2H), 1.74 (m, 2H), 1.33 (m, 12H), 0.87 (s, 3H). **¹³C NMR (126 MHz, CDCl₃, δ):** 144.23, 130.21, 129.80, 126.54, 116.75, 114.84, 47.71, 31.83, 29.29, 26.91, 26.74, 22.74, 14.22. **HRMS (ESI):** calculated for C₂₀H₂₃Br₂NS is 469.28 and found 469.9942 [M⁺].

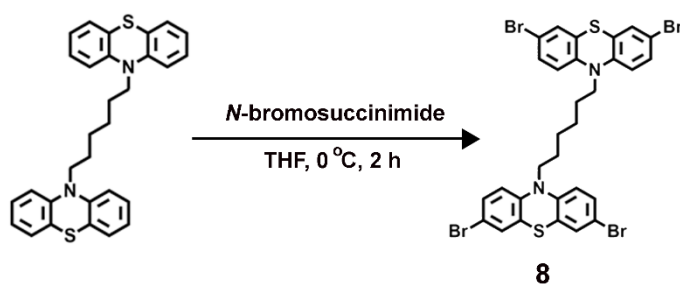


Scheme S8 Schematic illustration of the synthetic pathway of 1,6-di(10H-phenothiazine-10-yl)hexane (**7**).

Synthesis of 1,6-di(10H-phenothiazine-10-yl)hexane (7**):** 1,6-Di(10H-phenothiazine-10-yl)hexane was synthesized following a reported method with certain modifications (Scheme S8).³ Phenothiazine (2.0 mmol) and potassium *tert*-butoxide (3.2 mmol) were taken in a Schlenk tube. The N₂/vacuum cycle was carried out three times. After that, dry THF (10 mL) was added. The mixture was stirred at 25 °C for 12 h after the addition of 1,6-dibromohexane

(0.8 mmol) and quenched by adding water after completion of the reaction. The organic phase was extracted with dichloromethane, followed by drying over anhydrous sodium sulphate (Na_2SO_4). Silica gel column chromatography was performed to purify the residue after the solvent evaporation using hexane/dichloromethane (V/V, 8/2) as the eluent (72% yield, Scheme S8).

^1H NMR (500 MHz, CDCl_3 , δ): δ 7.13 (m, 8H), 6.90 (m, 4H), 6.82 (m, 4H), 3.81 (m, 4H), 1.81-1.75 (m, 4H), 1.45 (s, 4H). **^{13}C NMR (126 MHz, CDCl_3 , δ):** 145.33, 127.43, 127.17, 124.95, 122.33, 115.41, 47.32, 29.05, 26.80. **HRMS (ESI):** calculated for $\text{C}_{30}\text{H}_{28}\text{N}_2\text{S}_2$ is 480.17 and found 479.7780 [M^+].

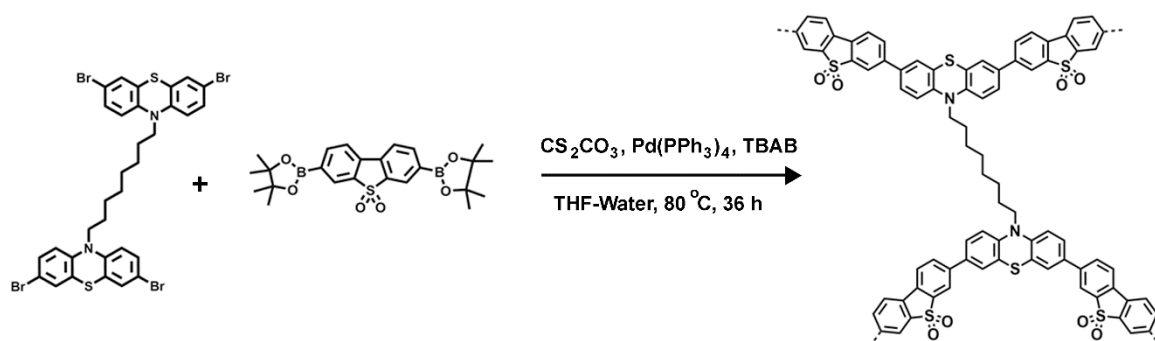


Scheme S9 Schematic illustration of the synthetic pathway of 1,6-bis(3,7-dibromo-10H-phenothiazine-10-yl)hexane (**8**).

Synthesis of 1,6-bis(3,7-dibromo-10H-phenothiazine-10-yl)hexane (BDPzH, **8):** 1,6-Bis(3,7-dibromo-10H-phenothiazine-10-yl)hexane was synthesized following a reported method with slight modification (Scheme S9).⁴ **7** (0.35 mmol) and *N*-bromo succinimide (NBS, 1.94 mmol) were taken in a Schlenk tube. The N_2 /vacuum cycle was carried out three times. After that, dry THF (10 mL) was added and stirred at 0 °C for 2 h. After completion of the reaction, water was added to quench it. Dichloromethane was added to extract the organic phase, followed by drying over anhydrous sodium sulphate (Na_2SO_4). Silica gel column chromatography was carried out to purify the residue after the solvent evaporation using hexane/dichloromethane (V/V, 9/1) as the eluent (37% yield, Scheme S9).

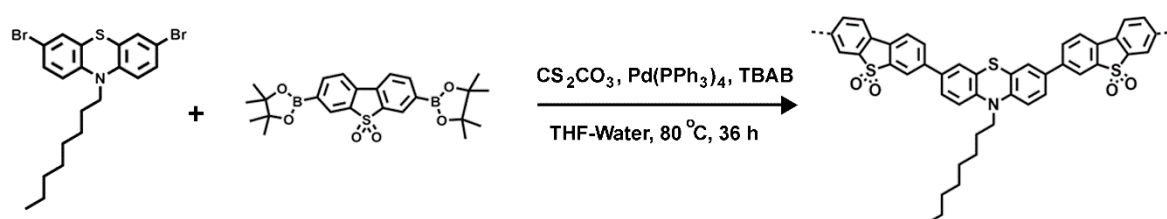
^1H NMR (500 MHz, CDCl_3 , δ): 7.24 (m, 8H), 6.66 (m, 4H), 3.76 (m, 4H), 1.73 (m, 4H), 1.41 (m, 4H). **^{13}C NMR (126 MHz, CDCl_3 , δ):** 144.15, 130.13, 129.76, 126.53, 116.72, 114.76, 47.42, 28.95, 26.54. **HRMS (ESI):** calculated for $\text{C}_{30}\text{H}_{24}\text{Br}_4\text{N}_2\text{S}_2$ is 796.27 and found 795.5510 [M^+].

(b) Synthesis of the soluble porous organic polymer (PzDBS), soluble linear organic polymer (PzBDS-L) and insoluble porous organic polymer (PzDBS-C):



Scheme S10 Synthetic pathways of PzDBS.

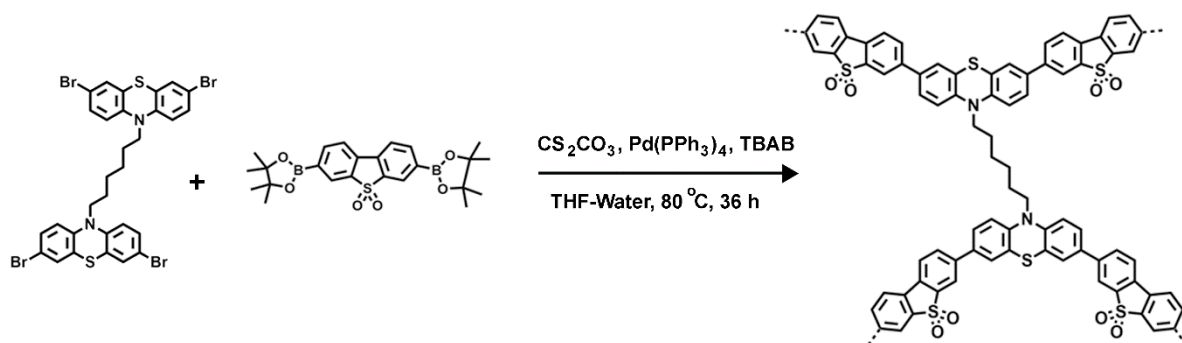
Fabrication of the soluble porous organic polymer (PzDBS): 1,8-Bis(3,7-dibromo-10H-phenothiazine-10-yl)octane (0.12 mmol), 3,7-bis(4,4,5,5-tetramethyl-1,3,2-dioxaborolan-2-yl)dibenzothiophene dioxide (0.3 mmol), and tetrabutylammonium bromide were taken in a Schlenk tube. N_2 /vacuum cycle was carried out three times. After that, tetrakis(triphenylphosphine)palladium (0) and dry THF (15 mL) was added, followed by freeze-pump-thaw cycles. Then, a deoxygenated cesium carbonate solution (2 mL, 2 M) was added, and the reaction was continued at 80°C for 36 h. After bringing the reaction mixture to room temperature, water was added to quench the reaction. Dichloromethane was used to extract the organic phase, followed by washing with 1 M hydrochloric acid. After that, an aqueous solution of sodium bicarbonate and EDTA was added. The organic phase was collected and dried by anhydrous Na_2SO_4 . Further, the residue was precipitated in cold methanol followed by filtration and final purification by Soxhlet extraction using methanol for 24 h (35 % yield, Scheme S10).



Scheme S11 Synthetic pathways of PzBDS-L.

Fabrication of the soluble linear polymer (PzBDS-L): 3,7-Dibromo-10-octyl-10H-phenothiazine (0.21 mmol), 3,7-bis(4,4,5,5-tetramethyl-1,3,2-dioxaborolan-2-yl)dibenzothiophene dioxide (0.25 mmol), and tetrabutylammonium bromide were taken in a Schlenk tube. N_2 /vacuum cycle was carried out three times. After that, tetrakis(triphenylphosphine)palladium (0) and dry THF (15 mL) was added, followed by freeze-pump-thaw cycles. Then, a deoxygenated cesium carbonate solution (2 mL, 2 M) was

added, and the reaction was continued at 80 °C for 36 h. After bringing the reaction mixture to room temperature, water was added to quench the reaction. Dichloromethane was used to extract the organic phase, followed by washing with 1 M hydrochloric acid. After that, an aqueous solution of sodium bicarbonate and EDTA was added. The organic phase was collected and dried by anhydrous Na₂SO₄. Further, the residue was precipitated in cold methanol followed by filtration and final purification by Soxhlet extraction using methanol for 24 h (47 % yield, Scheme S11).



Scheme S12 Synthetic pathways of PzDBS-C.

Fabrication of the insoluble porous organic polymer (PzDBS-C): 1,6-Bis(3,7-dibromo-10H-phenothiazine-10-yl)hexane (0.12 mmol), 3,7-bis(4,4,5,5-tetramethyl-1,3,2-dioxaborolan-2-yl) dibenzothiophene dioxide (0.3 mmol), and tetrabutylammonium bromide were taken in a Schlenk tube. The N₂/vacuum cycle was carried out three times. After that, tetrakis(triphenylphosphine)palladium (0) and dry THF (15 mL) was added, followed by freeze-pump-thaw cycles. Then, a deoxygenated cesium carbonate solution (2 mL, 2 M) was added, and the reaction was continued at 80 °C for 36 h. After bringing the reaction mixture to room temperature, acidified cold methanol was added to quench the reaction and was stirred for 30 min before filtration. The filtrate was washed several times using THF and chloroform and purified by Soxhlet extraction using methanol for 24 h (Scheme S12).

(c) Characterization of soluble porous organic polymer (PzDBS):

(i) Gel permeation chromatography (GPC) analysis:

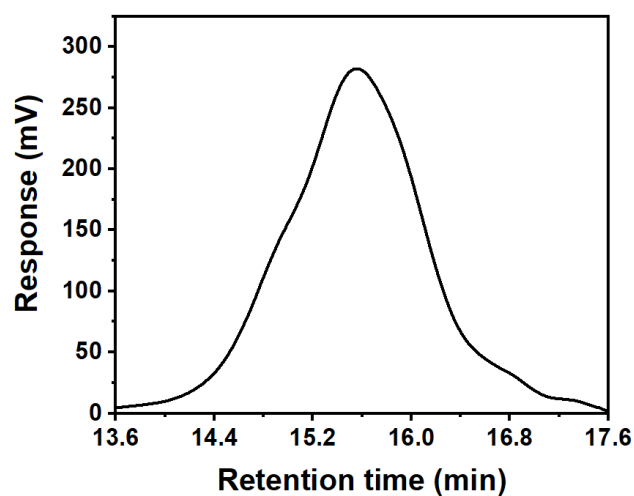


Fig. S1 GPC chromatogram of PzDBS.

(ii) Nuclear magnetic resonance (NMR) spectroscopy:

The similar resonances of PzDBS with respect to monomers (BDPzO, TDDBS), along with the other resonances, indicate the polycondensation reaction (Fig. S2).

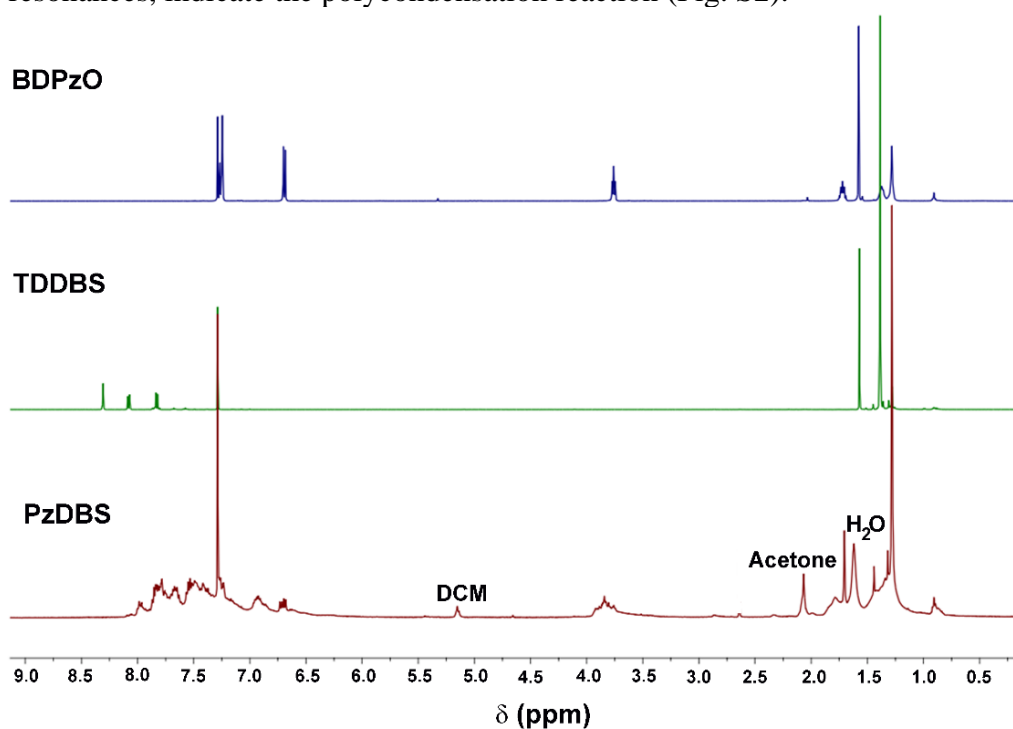


Fig. S2 ¹H NMR spectra of polymer PzDBS (red), TDDBS (green), and BDPzO (blue) in CDCl₃.

(iii) Fourier transform infrared (FTIR) spectroscopy:

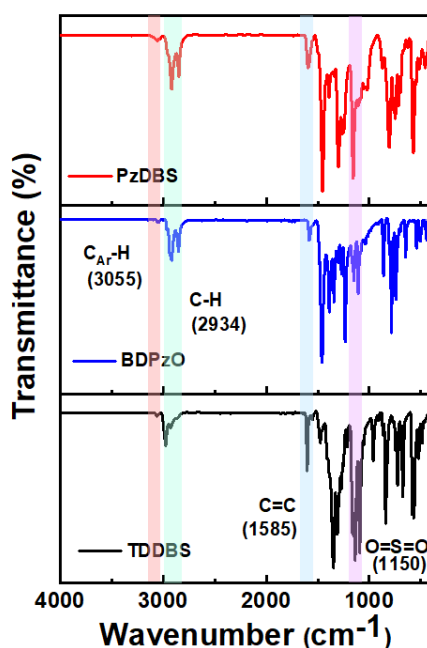


Fig. S3 FTIR spectra of PzDBS polymer (red), 1,8-bis(3,7-dibromo-10*H*-phenothiazin-10-yl)octane (BDPzO, blue) and 3,7-bis(4,4,5,5-tetramethyl-1,3,2-dioxaborolan-2-yl) dibenzothiophene dioxide (TDDBS, black).

(iv) Thermogravimetric analysis (TGA):

Little mass loss at around 100 °C was due to the evaporation of the trapped solvent molecules.

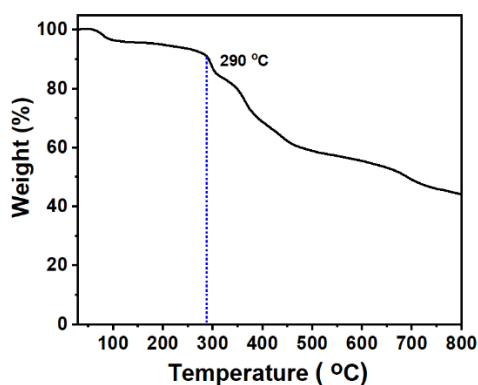


Fig. S4 TGA-plot of PzDBS.

(v) Selected area electron diffraction (SAED):

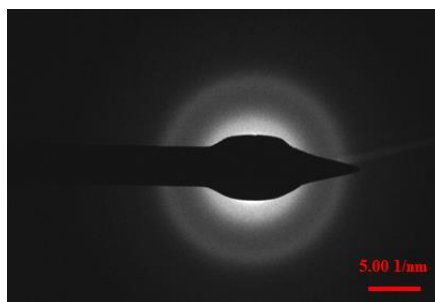


Fig. S5 SAED pattern of soluble porous organic polymer (PzDBS).

(vi) Elemental (CHNS) analysis:

The elemental composition of PzDBS was checked via CHNS analysis (Table S1). The idealized network structure was proposed from the elemental composition and the average molar mass obtained from gel permeation chromatography (GPC) analysis (Fig. S6). The deviation of the experimental elemental composition from the calculated one could be due to the trapped moisture, unreacted end groups, and oxygen present in the porous network (Fig. S4).⁶

Table S1 CHNS elemental analysis (calculated and experimental) of PzDBS.

Entry	C (wt%)		H (wt%)		N (wt%)		S (wt%)		O (wt%)	Br (wt%)
	Cal.	Expt.	Cal.	Expt.	Cal.	Expt.	Cal.	Expt.	Cal.	Cal.
PzDBS	69.90	67.10	4.17	4.43	2.45	2.95	13.68	11.67	8.05	1.75

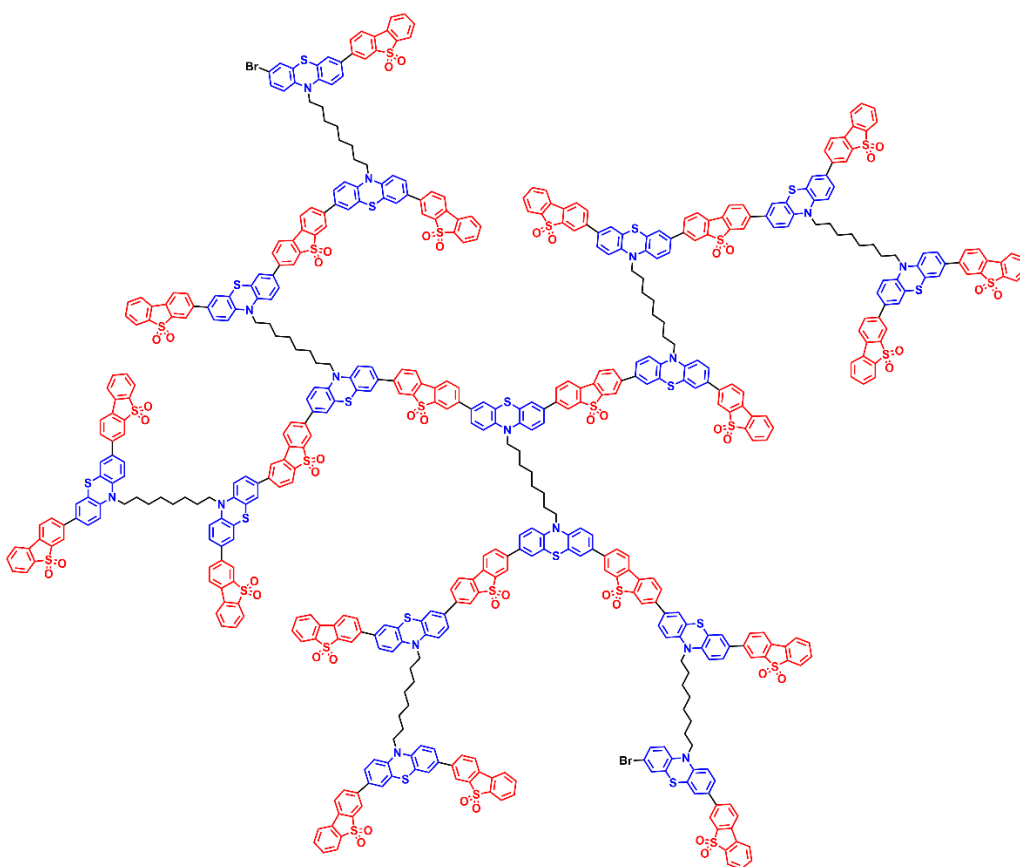


Fig. S6 Idealized polymer structure of PzDBS.

(d) Characterization of the soluble linear polymer (PzDBS-L):

(i) GPC analysis:

The weight average molar mass (M_w) of PzDBS-L was estimated to be $\sim 6260 \text{ g mol}^{-1}$ with a polydispersity index of 1.8 (Fig. S7) by GPC.

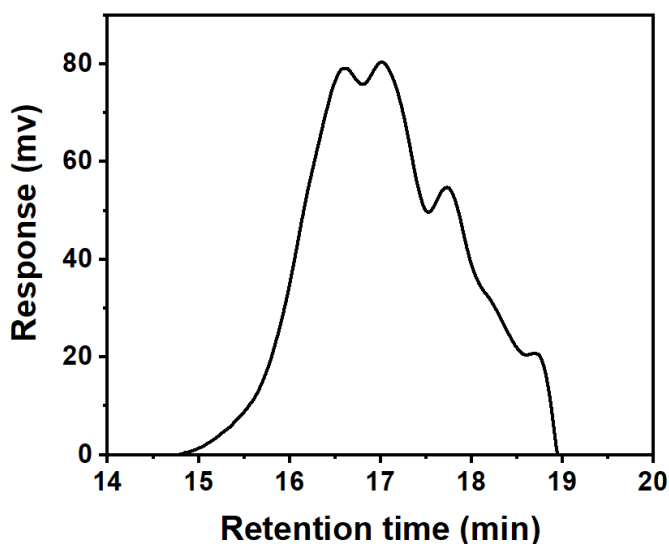


Fig. S7 GPC chromatogram of PzDBS-L.

(ii) Nuclear magnetic resonance (NMR) spectroscopy:

The similar resonances of PzDBS-L with respect to monomers, along with the other resonances, indicate the polycondensation reaction (Fig. S8).

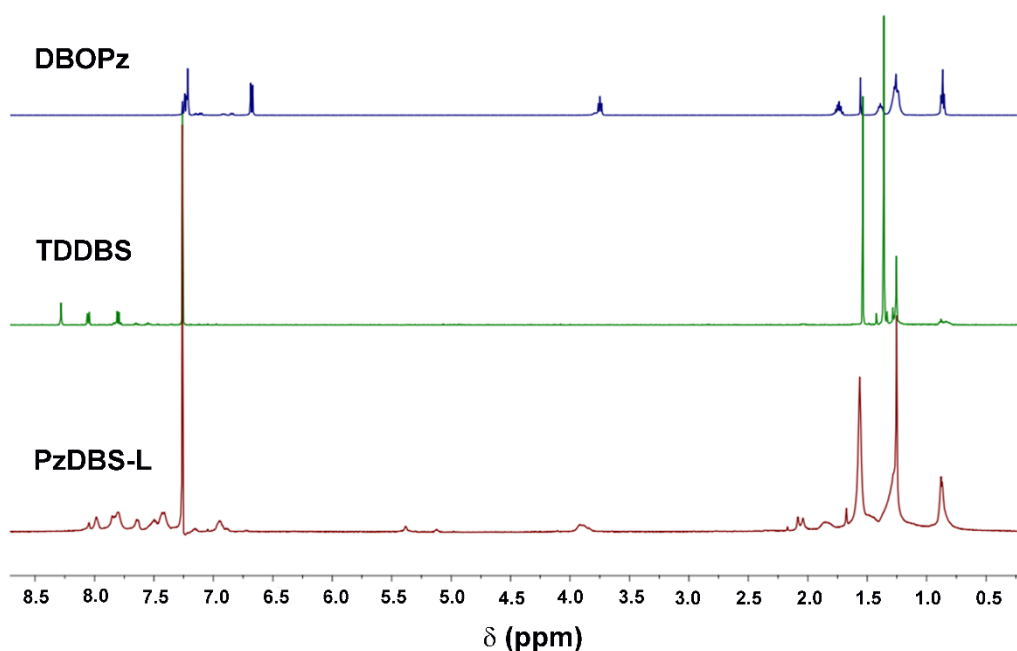


Fig. S8 ^1H NMR spectra of PzDBS-L (red), TDDBS (green) DBOPz (blue) in CDCl_3 .

(iii) Fourier transform infrared (FTIR) spectroscopy:

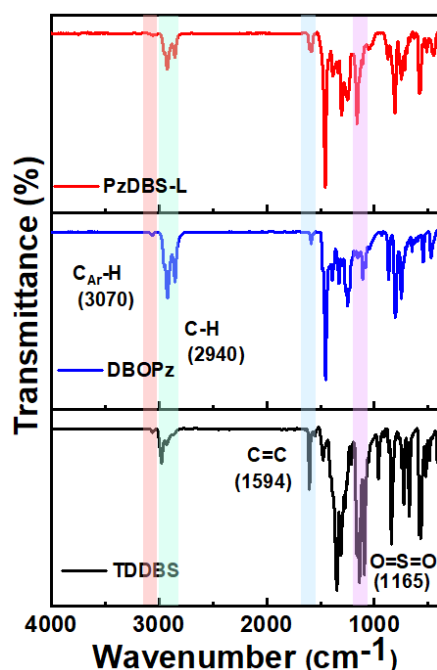


Fig. S9 FTIR spectra of PzDBS-L polymer (red), 3,7-dibromo-10-octyl-10*H*-phenothiazine (DBOPz, blue) and 3,7-bis(4,4,5,5-tetramethyl-1,3,2-dioxaborolan-2-yl) dibenzothiophene dioxide (TDDBS, black).

FTIR spectra of the linear polymer (PzDBS-L) and the monomers are shown in Fig. S9. The characteristic aromatic and aliphatic C–H stretching bands were observed, respectively, at 3070 cm⁻¹ and 2940 cm⁻¹ in both polymer and monomers. The peak at 1594 cm⁻¹ corresponded to C=C stretching, and the same was present in PzDBS-L and monomers. The peak at 1165 cm⁻¹ originated from the O=S=O group of dibenzothiophene dioxide unit present in PzDBS-L and the monomer, TDBDS.

(iv) Thermogravimetric analysis (TGA):

The thermogravimetric analysis of PzDBS-L suggested that the polymer was stable up to ~ 310 °C (Fig. S10).

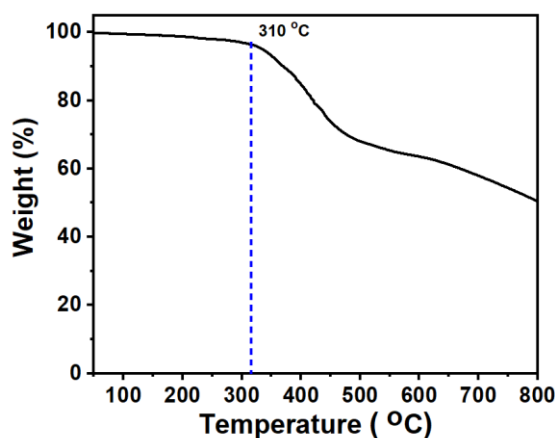


Fig. S10 TGA-plot of PzDBS-L.

IV. Microscopic characterization of PzDBS-L

(i) EFSEM of PzDBS-L:

The FESEM image showed the fused sphere-like morphology of PzDBS-L polymer (Fig. S11).

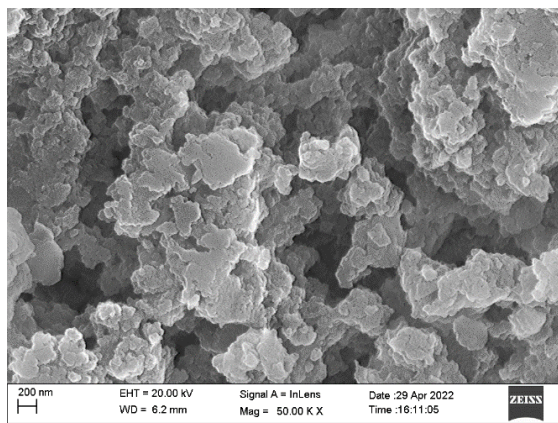


Fig. S11 FESEM image of PzDBS-L polymer.

(ii) HRTEM of PzDBS-L:

No lattice fringes were observed in the HRTEM images indicating a disordered amorphous structure of PzDBS-L (Fig. S12).

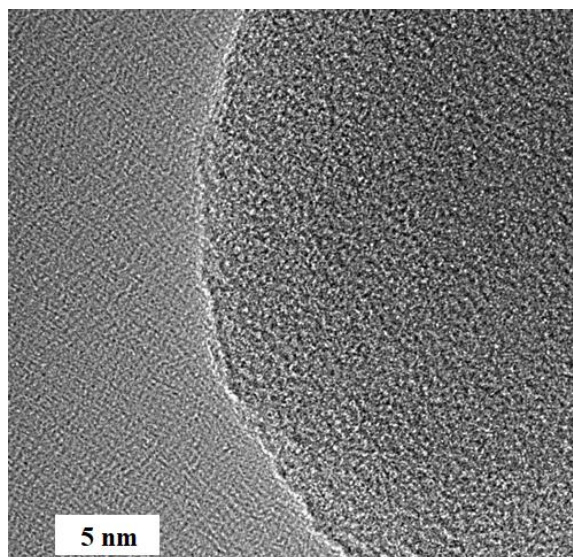


Fig. S12 HRTEM image of PzDBS-L polymer.

V. Surface area analysis of PzDBS-L

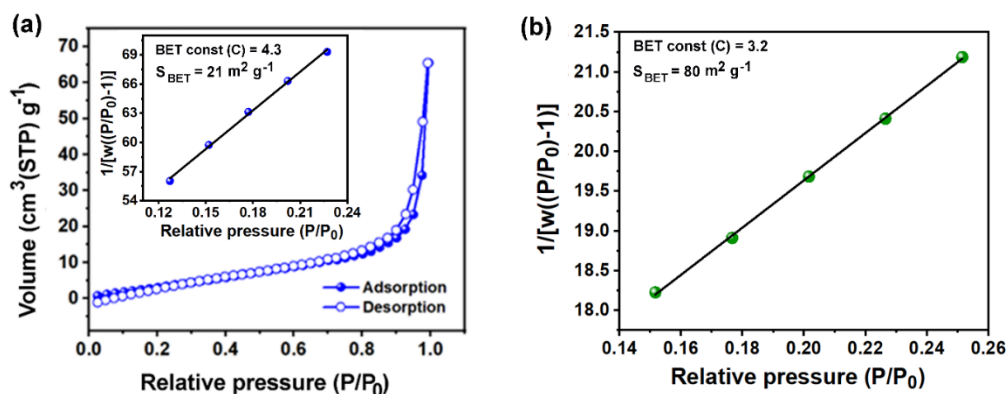


Fig. S13 (a) Nitrogen sorption isotherms of PzDBS-L polymer at 77 K. (b) BET linear plot of PzDBS.

VI. Characterization of PzDBS-C

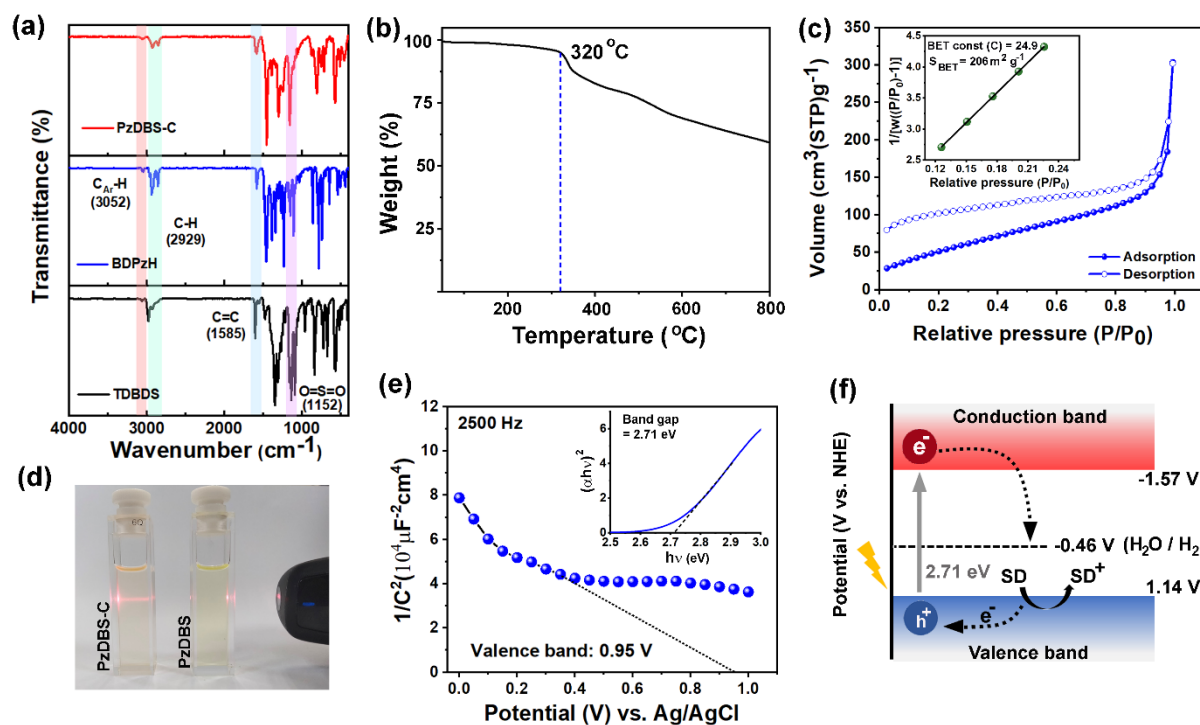


Fig. S14 (a) FTIR spectra of PzDBS-C polymer (red), 1,6-bis(3,7-dibromo-10*H*-phenothiazin-10-yl)hexane (BDPzH, blue) and 3,7-bis(4,4,5,5-tetramethyl-1,3,2-dioxaborolan-2-yl) dibenzothiophene dioxide (TDDBS, black). (b) TGA-plot of PzDBS-C. (c) Nitrogen sorption isotherms of PzDBS-C polymer at 77 K; inset: BET linear plot. (d) Optical images of PzDBS solution and PzDBS-C dispersion in dichloromethane indicating light scattering by PzDBS-C due to the heterogeneous colloidal medium. (e) Mott-Schottky analysis for the estimation of valence band energy of PzDBS-C; inset: Tauc plot for the estimation of the band gap. (f) Band diagram of PzDBS-C indicating the feasibility for photocatalytic hydrogen evolution similar to that of PzDBS; SD: sacrificial electron donor.

VII. Spectroscopic analysis of the PzDBS and PzDBS-L

The absorption spectra of PzDBS and PzDBS-L were compared with that of their precursor units (1,8-di(10H-phenothiazine-10-yl)octane and dibenzothiophene dioxide) in dichloromethane (Fig. S15). The main absorption peaks for PzDBS and PzDBS-L arising at 260-350 nm (π - π^* transition) were due to the phenothiazine and dibenzothiophene dioxide units, respectively. A broad absorption band at 385 and 404 nm was observed for PzDBS and PzDBS-L, respectively, due to the donor (11,8-di(10H-phenothiazine-10-yl)octane to an acceptor (dibenzothiophene dioxide) intramolecular charge transfer.^{7,8} No significant change in peak maxima and shape were found in the absorption spectra for both polymers with varying solvent polarity.

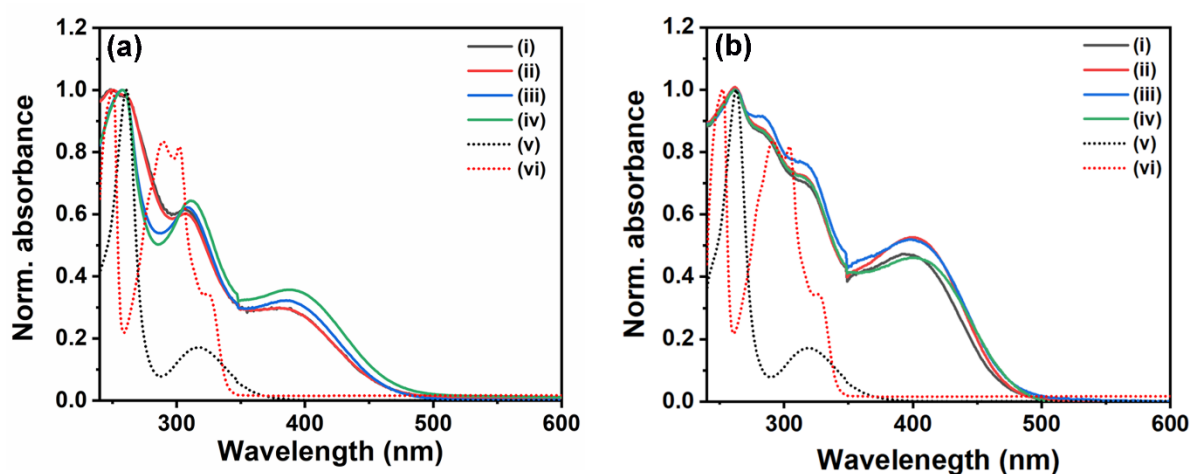


Fig. S15 Normalized absorption spectra of (a) PzDBS and (b) PzDBS-L in (i) toluene, (ii) dioxane, (iii) tetrahydrofuran, (iv) dichloromethane. Normalized absorption spectra (dotted line) of 1,8-di(10H-phenothiazine-10-yl)octane (v) and dibenzothiophene dioxide (vi) in dichloromethane are shown for comparison.

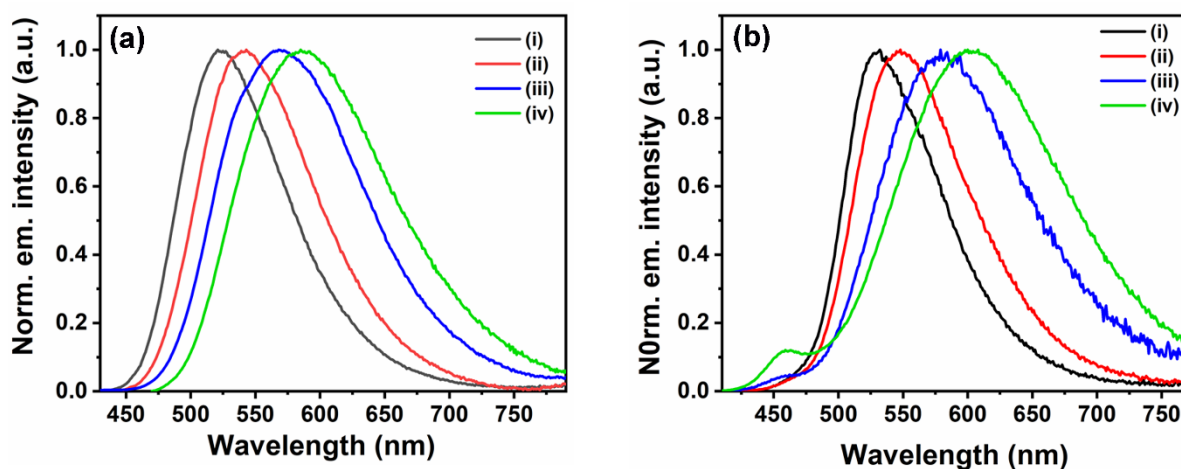


Fig S16. Normalized emission spectra of (a) PzDBS ($\lambda_{\text{ex}} = 380$ nm) and (b) PzDBS-L ($\lambda_{\text{ex}} = 400$ nm) in (i) toluene, (ii) dioxane, (iii) tetrahydrofuran, and (iv) dichloromethane.

The significant Stokes shifts and spectral broadening in the polar solvents indicated a highly polar ICT state (Table S2, Fig. S16).^{9,10,11}

Table S2 Solvent polarity parameters (E_T^N), dielectric constants (ϵ), refractive indices (n), orientation polarizabilities (Δf) of different solvents, and the Stokes shift (nm) of PzDBS and PzDBS-L are shown.

Entry	Solvents				Stokes shift (nm)	
	E_T^N	ϵ	n	Δf	PzDBS	PzDBS-L
Toluene	0.099	2.38	1.50	0.013	133	124
1,4-dioxane	0.164	2.25	1.42	0.024	153	142
Tetrahydrofuran	0.207	7.58	1.41	0.210	179	174
Dichloromethane	0.309	8.93	1.42	0.217	199	196

VIII. Electrochemical studies of PzDBS and PzDBS-L

Cyclic voltammetry of ferrocene was carried out for calibration of the instrument. The half-cell potential of ferrocene-ferrocenium (FC/FC⁺) was found to be 0.50 V vs. Ag/AgCl (Fig. S17). Cyclic voltammetry of PzDBS and PzDBS-L was carried out to estimate the valence band position (Fig. S18). The half-cell potentials ($E_{1/2}$) were used to calculate the valence band (VB) according to the following equation: $VB = - \left(E_{\frac{1}{2}, OX} + 4.8 - E_{\frac{1}{2}, FC/FC+} \right) eV \dots \dots \dots (i)$ ¹². Conduction band energy (CB) of both the polymers was estimated using the following equation: CB: Band gap + VB.....(ii) (Fig. S19). The band gap of both the polymers (PzDBS: 2.76 eV, PzDBS-L: 2.57 eV) was estimated from the Tauc plot.

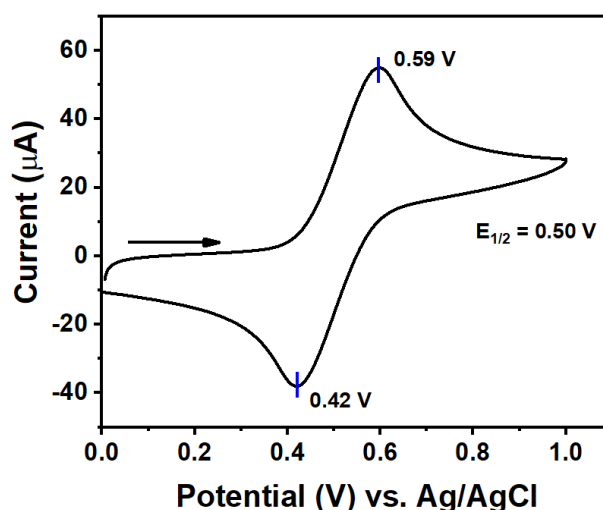


Fig. S17 Cyclic voltammogram of ferrocene.

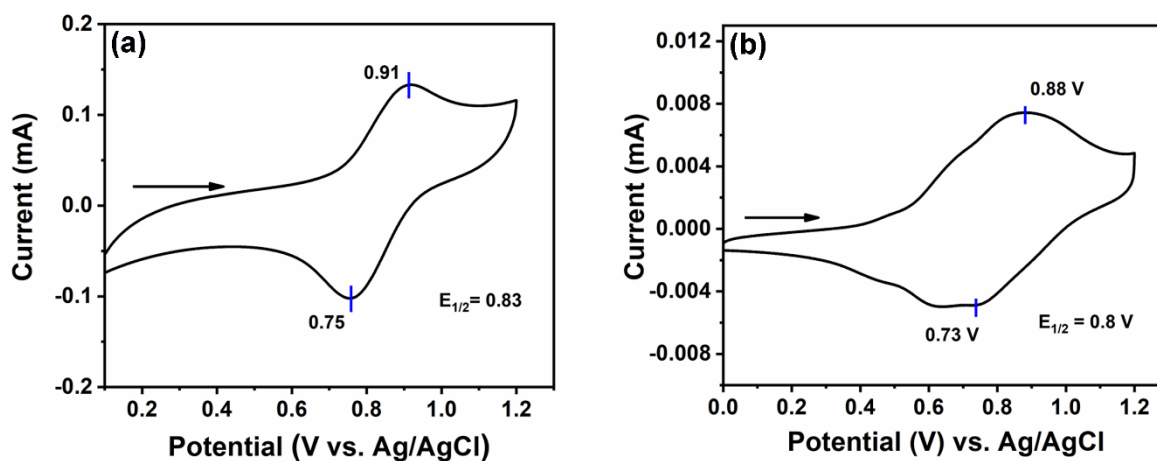


Fig. S18 Cyclic voltammogram of (a) PzDBS and (b) PzDBS-L.

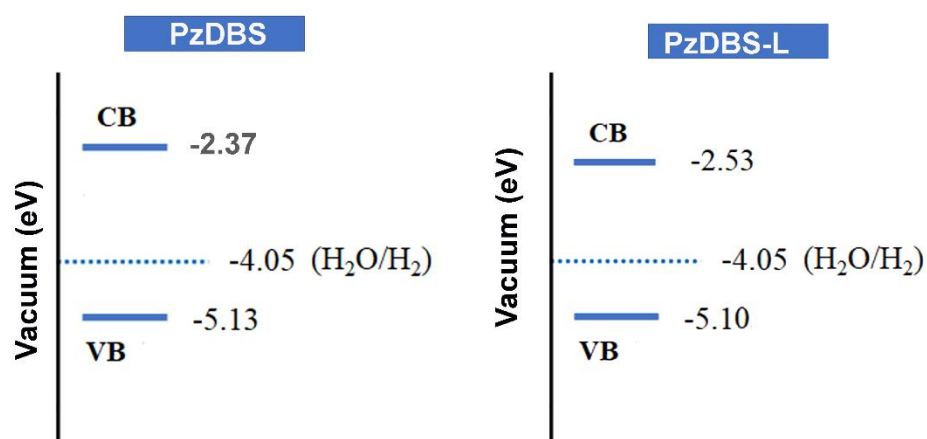


Fig. S19 Band energy diagram of PzDBS and PzDBS-L in vacuum scale calculated via cyclic voltammetry and Tauc plot indicating the possibility of photocatalytic hydrogen evolution via transferring the electron from the conduction band of the polymer (PzDBS/PzDBS-L) to water.

IX. Calibration curve for the estimation of evolved hydrogen

A standard H₂/N₂ gas mixture (V/V, 10/90) was used as the calibration reference for the gas chromatography, where N₂ was used as a carrier gas, and a thermal conductivity detector (TCD) was used for the H₂ detection (Fig. S20). Fig. S21 indicated the evolved hydrogen after photocatalytic reaction using PzDBS in a biphasic system in the presence of triethylamine as a sacrificial reducing agent upon 300 W Xe lamp irradiation (290-1800 nm) for 8 h.

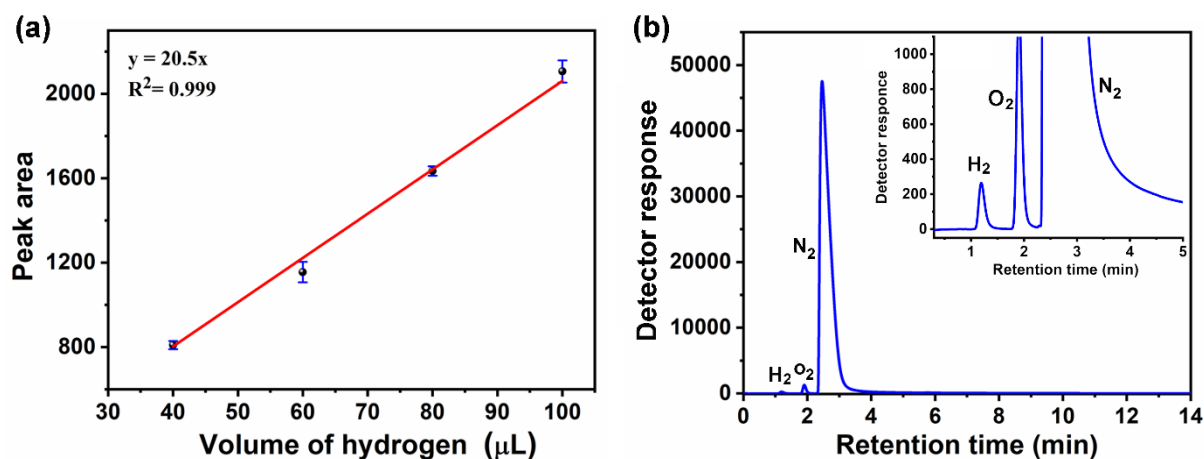


Fig. S20 (a) Calibration curve for estimating evolved hydrogen in photocatalysis reaction. (b) Gas chromatogram of 1 mL standard H₂/N₂ gas mixture (100 μL H₂).

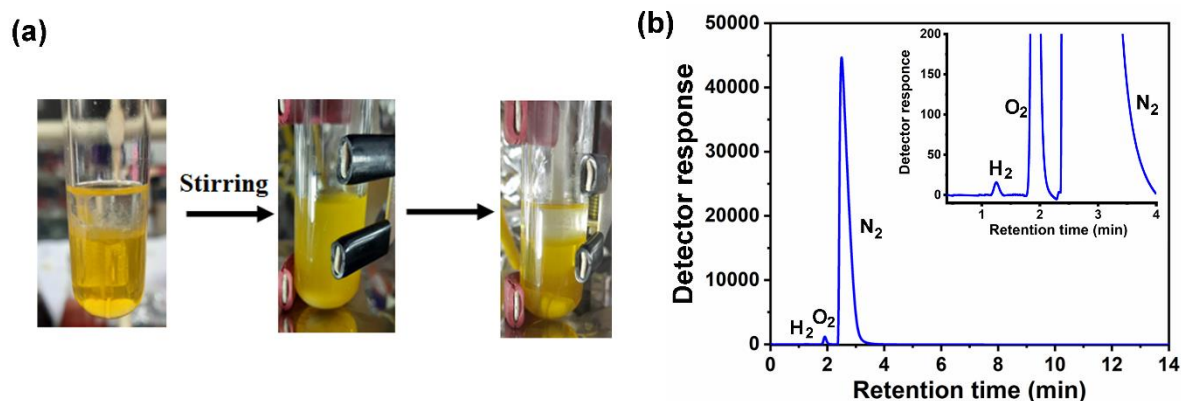


Fig. S21 (a) Digital images of the biphasic photocatalytic hydrogen evolution set-up, where DCM containing PzDBS constitutes the organic phase, water acts as an aqueous phase, and triethylamine as a sacrificial electron donor. (b) Gas chromatogram of 1 mL headspace gases generated after the biphasic photocatalytic reaction using PzDBS for 8 h suggesting the generation of hydrogen gas (retention time 1.2 s).

X. Optimization of the photocatalytic reaction conditions

Mott–Schottky analysis of PzDBS was performed in the presence of triethylamine and ascorbic acid to check the change in the energy band position. The valance band (VB) and conduction band (CB) of PzDBS were positioned at 0.99 V and -1.77 V vs. NHE in the presence of triethylamine (VB: 0.8 V vs. Ag/AgCl, CB: -1.96 V vs. Ag/AgCl, Fig. S23a, S24). Whereas the VB and CB of PzDBS were positioned at 1.65 V and -1.11 V vs. NHE in the presence of ascorbic acid (VB: 1.46 V vs. Ag/AgCl, CB: -1.3 V vs. Ag/AgCl, Fig. S23b, S24). The higher conduction band position (-1.77 V vs. NHE) in the presence of triethylamine (TEA) compared to -1.11 V vs. NHE in the presence of ascorbic acid suggests the higher photocatalytic rate of PzDBS in the presence of TEA.¹³ Moreover, the lower potential difference between the conduction band and substrate molecule (water) in the case of ascorbic acid (potential difference: 0.96 V vs. NHE, Fig. S24) led to a lower hydrogen evolution activity compared to TEA (potential difference: 1.07 V vs. NHE, Fig. S24). The rate of the biphasic photocatalytic hydrogen evolution was found to be the highest ($494 \pm 24 \mu\text{mol g}^{-1} \text{h}^{-1}$) for 2 h in TEA. However, a slight decrease ($367 \pm 25 \mu\text{mol g}^{-1} \text{h}^{-1}$) in activity was observed after 8 h due to the aggregation of PzDBS after prolonged water contact, which was supported by SEM characterization before and after photocatalysis (Fig. S25).

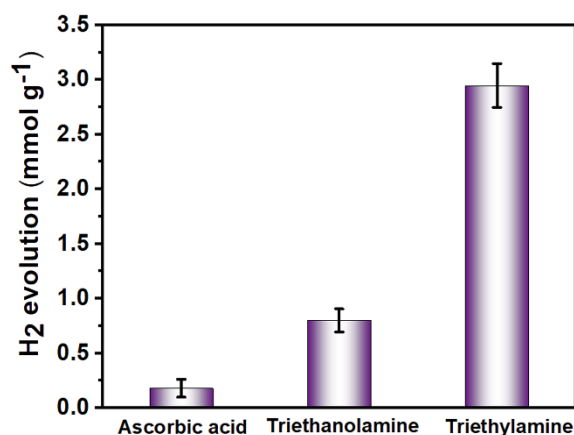


Fig. S22 Biphasic photocatalytic H₂ evolution using different sacrificial electron donors for PzDBS catalyst under light irradiation for 8 h; the bars represent standard deviation based on three independent measurements.

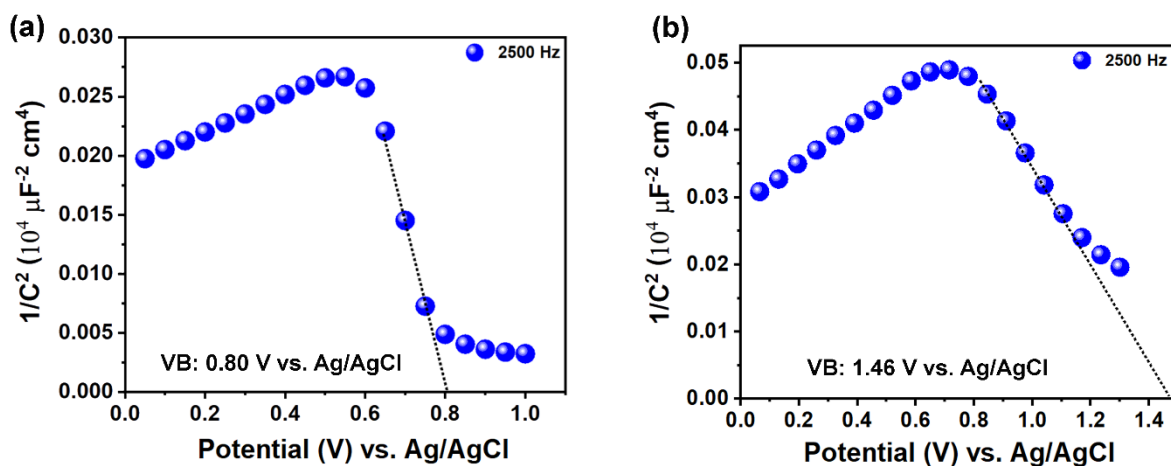


Fig. S23 Mott-Schottky analysis for the estimation of the valence band energy of PzDBS in the presence of (a) triethylamine, and (b) ascorbic acid.

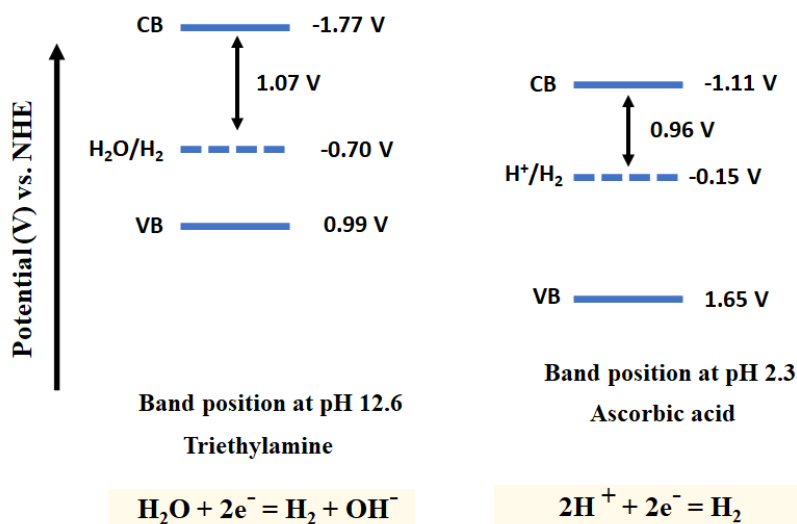


Fig. S24 Band diagram of PzDBS in the presence of triethylamine (left) and ascorbic acid (right).

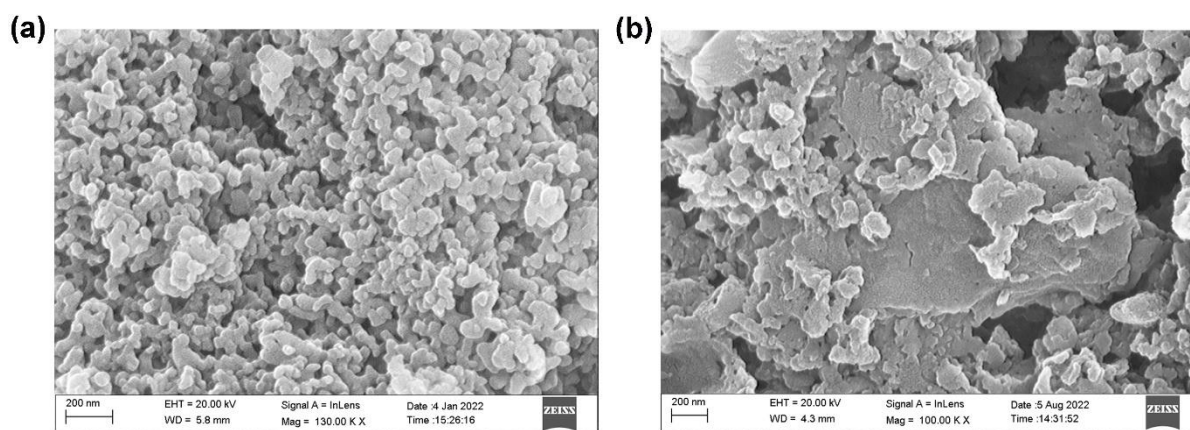


Fig. S25 FESEM images of PzDBS (a) before and (b) after reaction for 8 h in an aqueous-organic biphasic medium.

XI. Photocatalytic hydrogen evolution: biphasic vs. heterogeneous

Similar photocatalytic activity with the higher catalyst amount in the biphasic route ($367 \pm 25 \mu\text{mol g}^{-1} \text{h}^{-1}$ to $332 \pm 6 \mu\text{mol g}^{-1} \text{h}^{-1}$) compared to a gradual decrease in activity through the heterogeneous route ($259 \pm 15 \mu\text{mol g}^{-1} \text{h}^{-1}$ to $174 \pm 5 \mu\text{mol g}^{-1} \text{h}^{-1}$) indicates the advantage of the biphasic strategy (Fig. S26b).

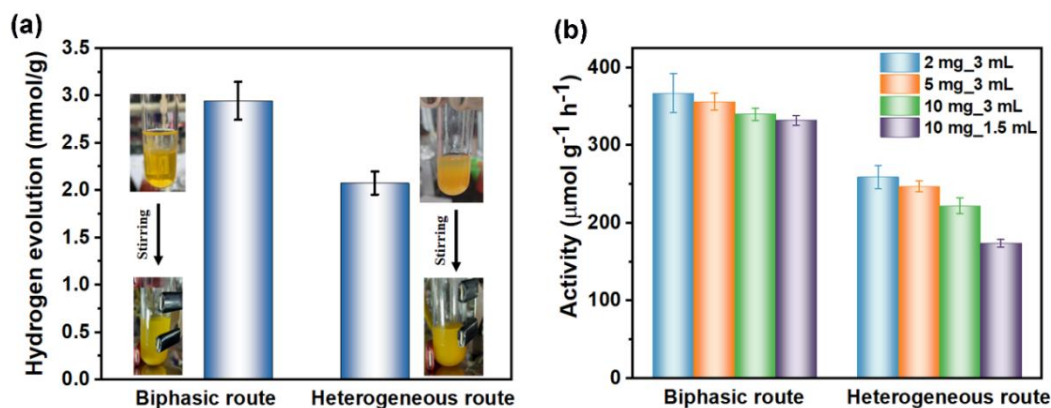


Fig. S26 (a) Photocatalytic hydrogen evolution of PzDBS (2 mg) in an aqueous-organic biphasic (water: DCM: TEA = 1: 1: 1) and heterogeneous (water: TEA = 1: 1) conditions upon Xe lamp irradiation for 8 h; inset: digital photographs of the corresponding reaction set-up. (b) H_2 evolution activity of PzDBS by varying the catalyst/water ratio in biphasic and heterogeneous route under the Xe lamp irradiation ($\lambda > 290 \text{ nm}$) for 8 h; the bars represent standard deviation based on three (for 2 mg of catalyst) and two (for 5 and 10 mg of catalyst) independent measurements.

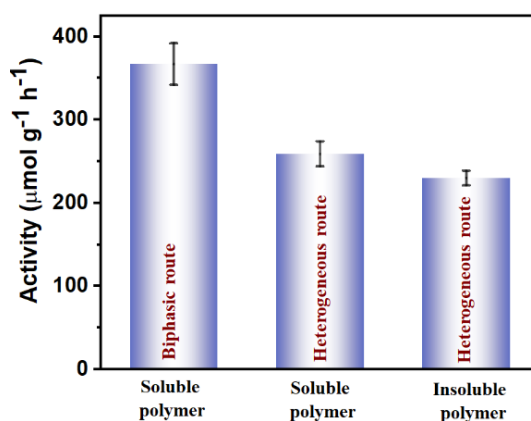


Fig. S27 H_2 evolution activity of soluble PzDBS (biphasic and heterogeneous route) and insoluble PzDBS-C (heterogeneous route) under Xe lamp irradiation ($\lambda > 290 \text{ nm}$) for 8 h; the bars represent standard deviation based on three independent measurements.

Further, the photocatalytic activity of soluble PzDBS was compared with the insoluble hexyl-linked PzDBS-C polymer in the heterogeneous medium (water: TEA = 1:1). The photocatalytic hydrogen evolution activity of PzDBS-C ($230 \pm 9 \mu\text{mol g}^{-1} \text{h}^{-1}$ after 8 h) was found to be similar to that of PzDBS when photocatalysis was performed through heterogeneous route ($259 \pm 15 \mu\text{mol g}^{-1} \text{h}^{-1}$ after 8 h) owing to the comparable band energy position and D-A structures (Fig.

S27, S14f). However, the photocatalytic hydrogen evolution activity of PzDBS in the biphasic route (water: DCM: TEA = 1: 1: 1) was found to be higher ($367 \pm 25 \mu\text{mol g}^{-1} \text{h}^{-1}$ after 8 h) than the heterogeneous route using PzDBS-C ($230 \pm 9 \mu\text{mol g}^{-1} \text{h}^{-1}$ after 8 h) and PzDBS ($259 \pm 15 \mu\text{mol g}^{-1} \text{h}^{-1}$ after 8 h).

XII. Contact angle measurement of PzDBS and PzDBS-L

The water wettability of PzDBS and PzDBS-L was investigated through contact angle measurements. The contact angle of PzDBS was found to be $\sim 89^\circ$, indicating the hydrophilic nature of the polymer (Fig. S28). On the other hand, the hydrophilic nature of PzDBS-L was less than the PzDBS, as indicated by the higher contact angle of PzDBS-L ($\sim 99^\circ$).

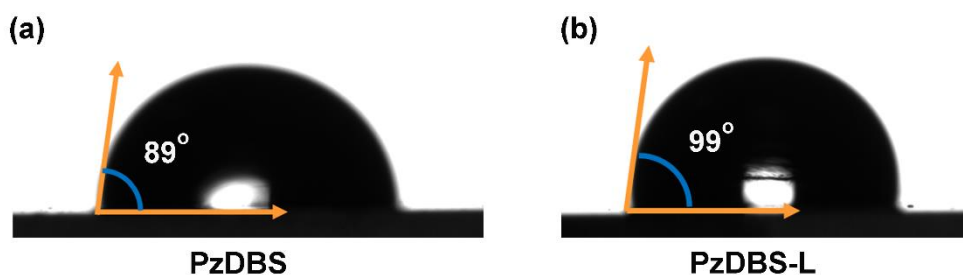


Fig. S28 Water contact angle of (a) PzDBS and (b) PzDBS-L.

XIII. Absorption and FTIR of the recycled catalyst (PzDBS)

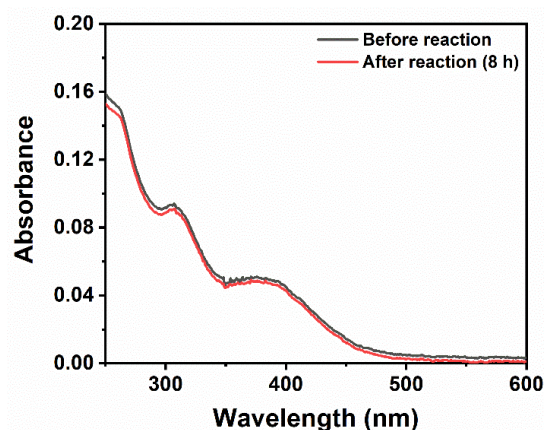


Fig. S29 Absorption spectra of PzDBS before and after photocatalytic reaction for 8 h.

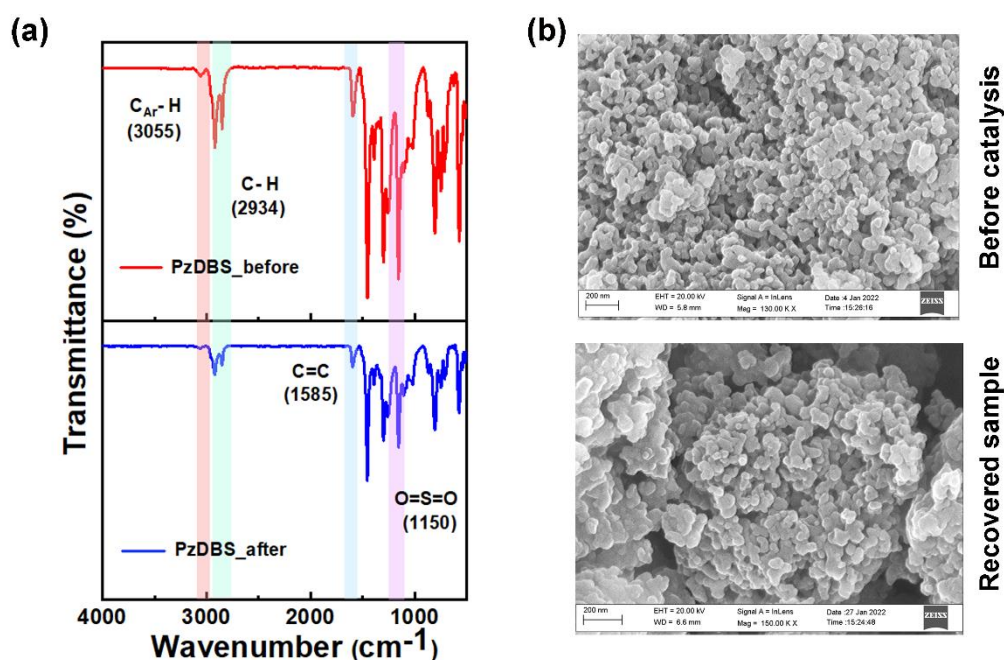


Fig. S30 (a) FTIR spectra and (b) FESEM images of PzDBS polymer before (top) and after photocatalysis reaction (below).

XIV. ICP-OES analysis

The inductively coupled plasma optical emission spectroscopy (ICP-OES) analysis was carried out for accurate estimation of the residual palladium present in the polymer synthesized by the Suzuki–Miyaura coupling reaction. Polymer (PzDBS and PzDBS-L) was digested for 24 h in 5 mL of aqua regia. Further, the samples were diluted by adding 25 mL of Milli Q water. The ICP-OES analysis confirmed the presence of the minimal amount of 0.38 wt% Pd in PzDBS and 0.53 wt% in PzDBS-L.

XV. Steady-state emission and lifetime analysis

The fluorescence intensity of PzDBS was found to be lower compared to PzDBS-L (Fig. S31a). The following equation (iii) was used to correct the intensities for the inner filter effect

$$I = I_{abs} * \text{antilog} (A_{ex} + A_{em}) / 2 \quad \dots(\text{iii})$$

Where, A_{ex} and A_{em} are the absorbance at excitation and emission wavelengths ($\lambda_{ex} = 385$ nm and $\lambda_{em} = 584$ nm for PzDBS; $\lambda_{ex} = 404$ nm and $\lambda_{em} = 600$ nm for PzDBS-L), respectively.

The fluorescence quantum yield of PzDBS and PzDBS-L in dichloromethane was calculated using coumarin 153 dye in ethanol ($\Phi_f = 38\%$) as the reference dye using the below equation.¹⁴

$$\Phi_{f,x} = \Phi_{f,s} * \frac{F_x}{F_s} * \frac{f_s}{f_x} * \frac{n_x^2}{n_s^2} \quad \dots (\text{iv})$$

Where Φ_f is the quantum yield of the fluorophore, and x and s refer to the sample and standard, respectively. F represents integral fluorescence. n is the refractive index of the solvent. The equation below provides the absorption factor (f) at the excitation wavelength.

$$f = 1 - 10^{-\varepsilon(\lambda_{ex})cl} = 1 - 10^{-A(\lambda_{ex})} \quad \dots \quad (v)$$

A = absorbance and ε = molar extinction coefficient ($M^{-1} \text{ cm}^{-1}$).

The fluorescence quantum yields of PzDBS and PzDBS-L were found to be 11 % and 17 %, respectively (Table S3).

Both the porous (PzDBS) and linear polymer (PzDBS-L) exhibited a biexponential fluorescence decay in dichloromethane due to the emission from the locally excited and charge transfer state (Fig. S31b).

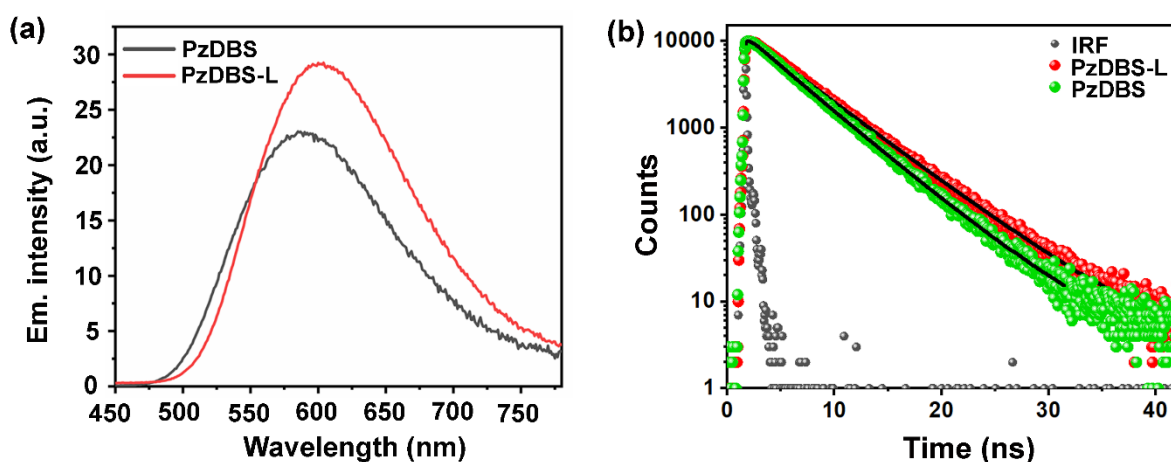


Fig. S31 (a) Emission spectra of PzDBS ($\lambda_{ex} = 385 \text{ nm}$) and PzDBS-L ($\lambda_{ex} = 404 \text{ nm}$) in dichloromethane. (b) Fluorescence decay profiles of PzDBS ($\lambda_{ex} = 405 \text{ nm}$) and PzDBS-L ($\lambda_{ex} = 405 \text{ nm}$) in dichloromethane.

Table S3 Spectroscopic data of PzDBS and PzDBS-L in dichloromethane; lifetime (ns) and the quality of fitting (χ^2) for the data are shown.

Entry	Abs λ_{abs} (nm)	FL λ_{em} (nm)	QY %	Lifetime (ns) ($\lambda_{ex} = 405 \text{ nm}$)					
				τ_1	α_1	τ_2	α_2	τ_{av}	(χ^2)
PzDBS	385	584	11	3.4	58.1	4.7	41.9	3.9	1.08
PzDBS-L	404	600	17	4.2	55.2	5.4	44.7	4.7	1.15

XVI. Computational investigation

The ground state geometries of the model structure of PzDBS and PzDBS-L were optimized by the density functional theory [B3LYP, 6-31G(d,p)]. The polarizable continuum model (PCM) was employed for all the calculations using the dielectric constant of DCM. GaussView 5.0 was used to analyze the computational data.

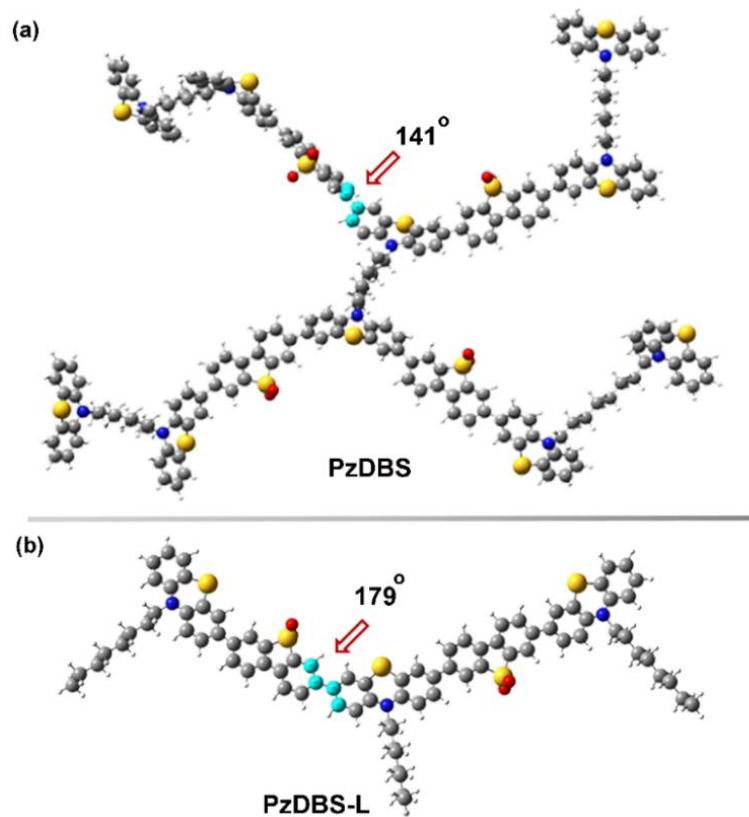


Fig. S32 DFT geometry optimized structures and dihedral angles of the repeating units of PzDBS and PzDBS-L.

XVII. Characterization: ^1H NMR, ^{13}C NMR and Mass spectra

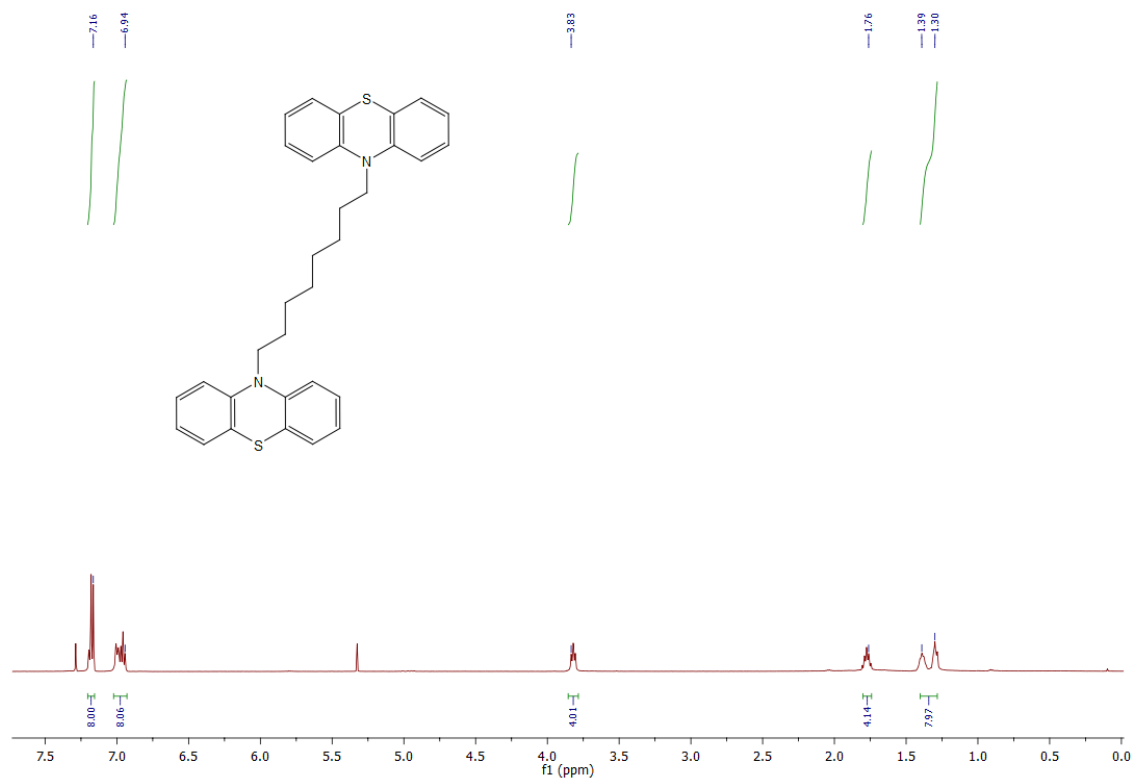


Fig. S33 ^1H NMR spectrum of 1,8-di(10H-phenothiazin-10-yl)octane (1) in CDCl_3 .

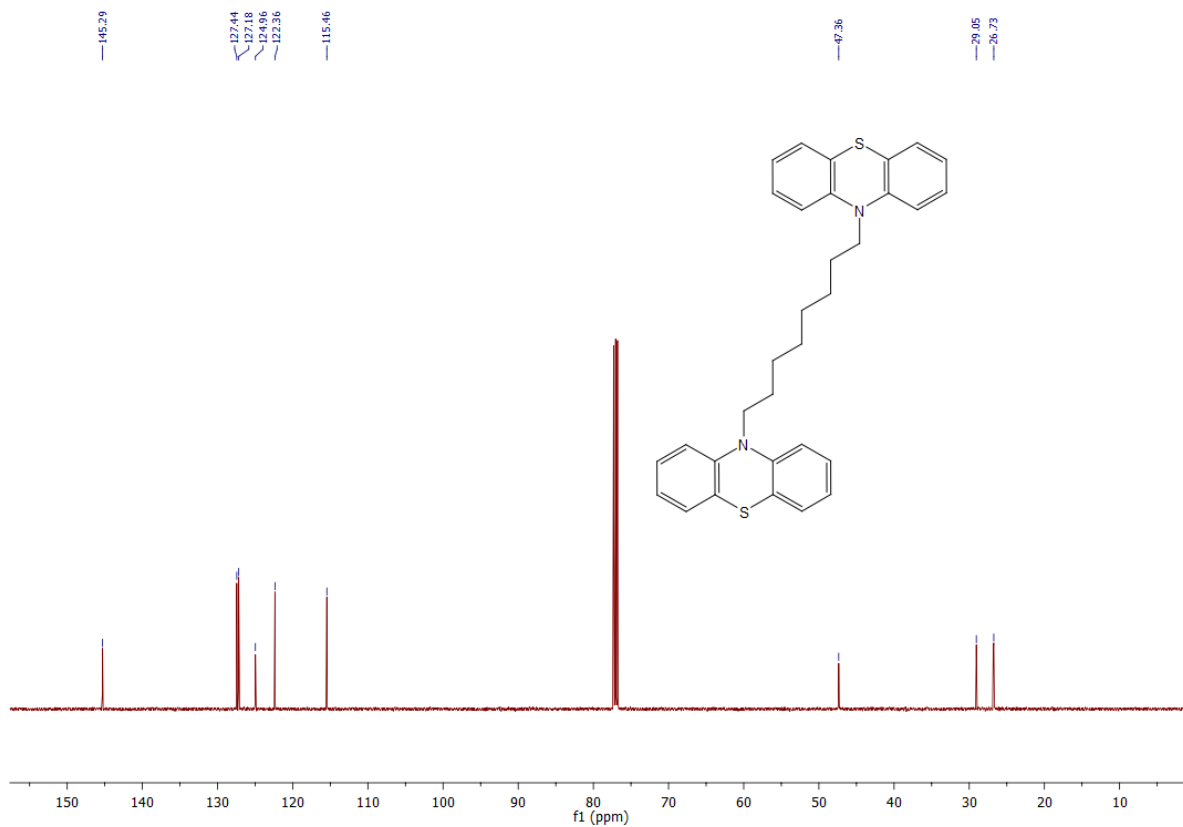


Fig. S34 ^{13}C NMR spectrum of 1,8-di(10H-phenothiazin-10-yl)octane (1) in CDCl_3 .

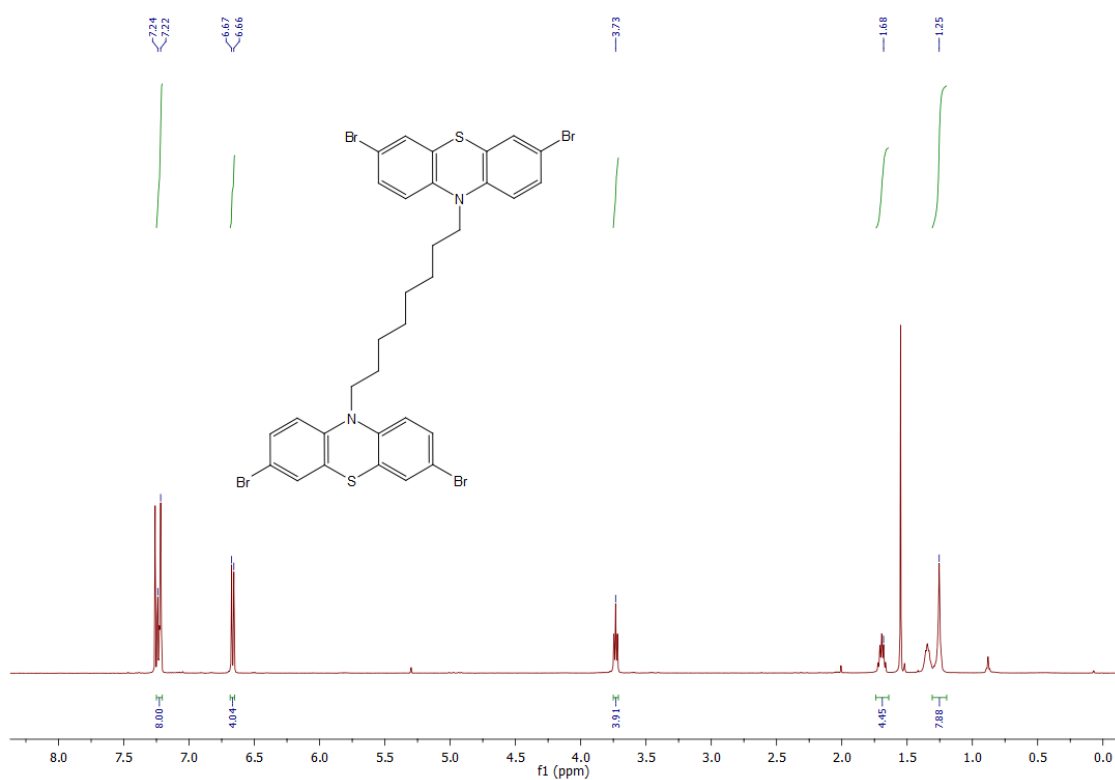


Fig. S35 ^1H NMR spectrum of 1,8-bis(3,7-dibromo-10H-phenothiazin-10-yl)octane (**2**) in CDCl_3 .

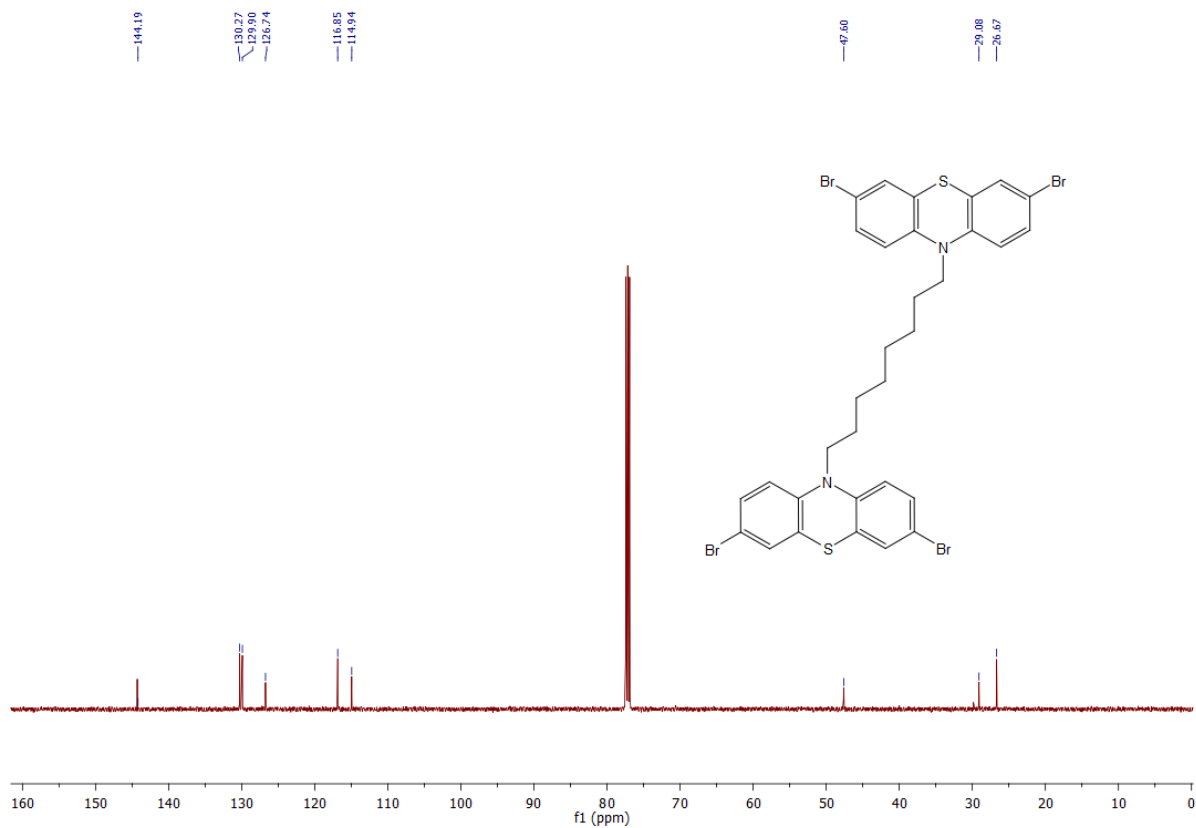


Fig. S36 ^{13}C NMR spectrum of 1,8-bis(3,7-dibromo-10H-phenothiazin-10-yl)octane (**2**) in CDCl_3 .

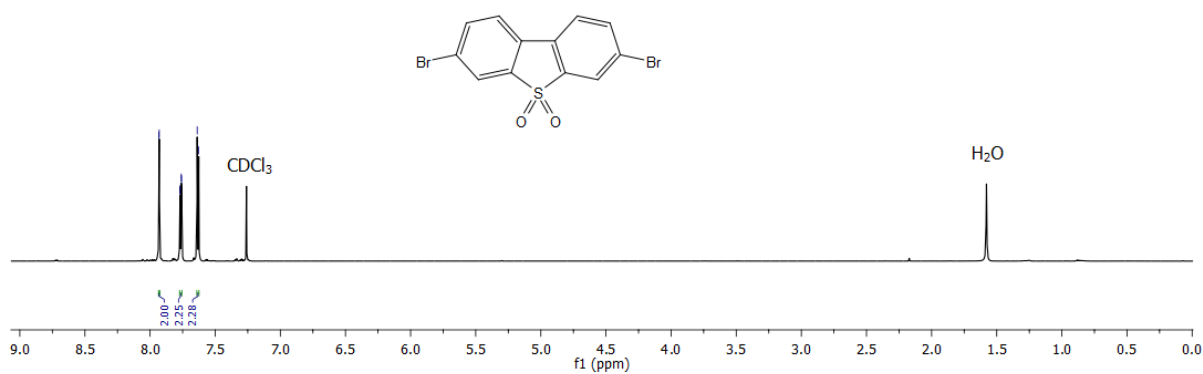
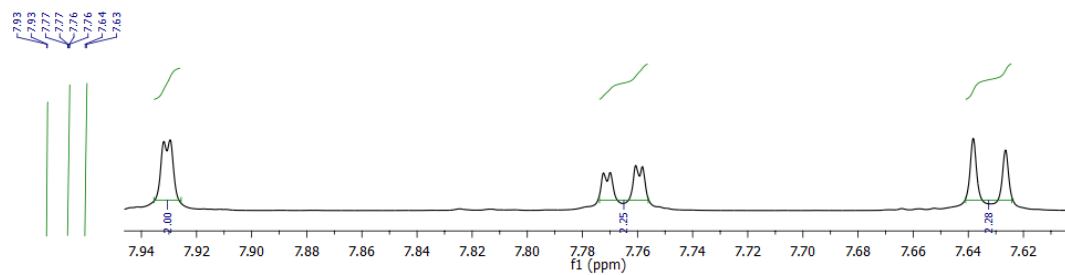


Fig. S37 ^1H NMR spectrum of 3,7-dibromodibenzo[b,d]thiophene 5,5-dioxide (**3**) in CDCl_3 .

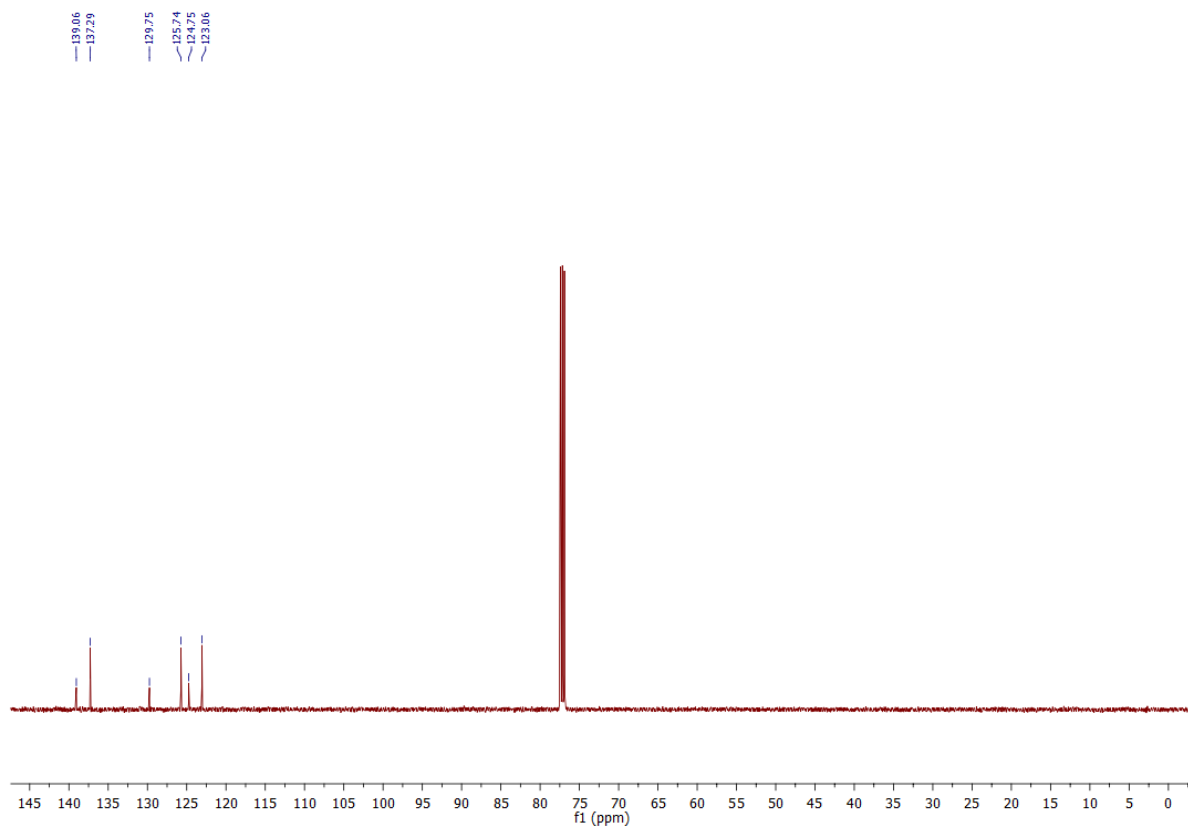


Fig. S38 ^{13}C NMR spectrum of 3,7-dibromodibenzo[b,d]thiophene 5,5-dioxide (**3**) in CDCl_3 .

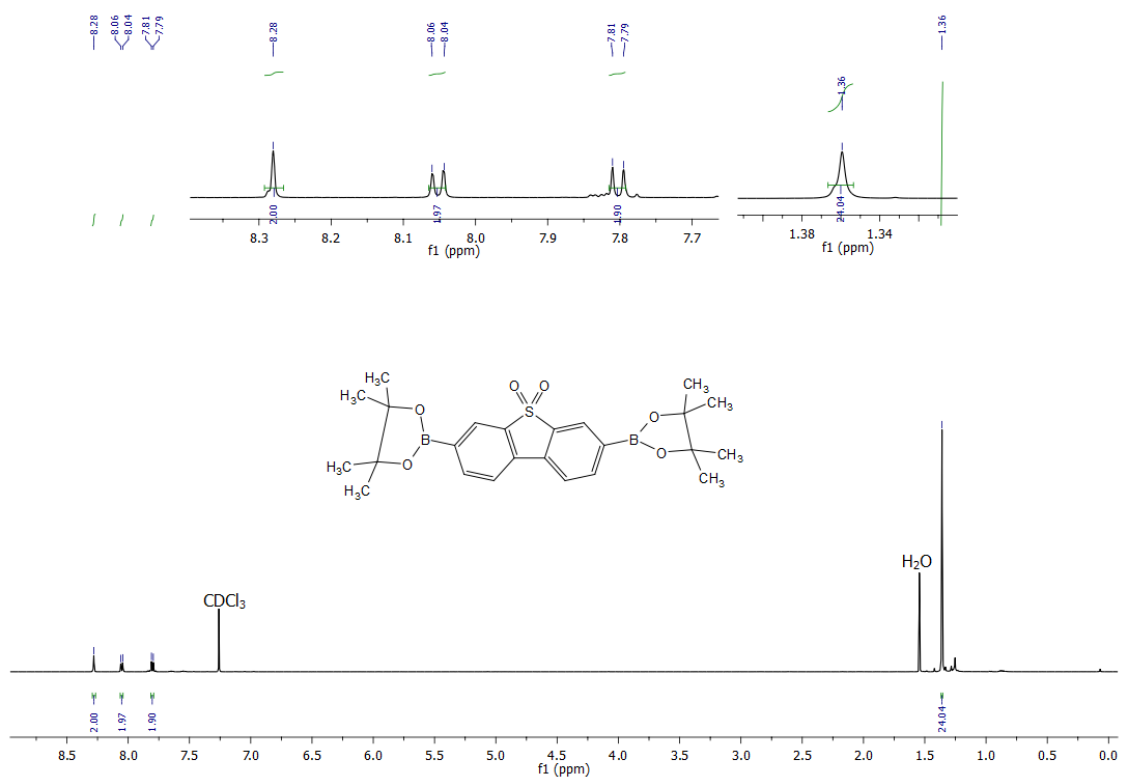


Fig. S39 ¹H NMR spectrum of 3,7-bis(4,4,5,5-tetramethyl-1,3,2-dioxaborolan-2-yl)dibenzo[b,d]thiophene 5,5-dioxide (**4**) in CDCl₃.

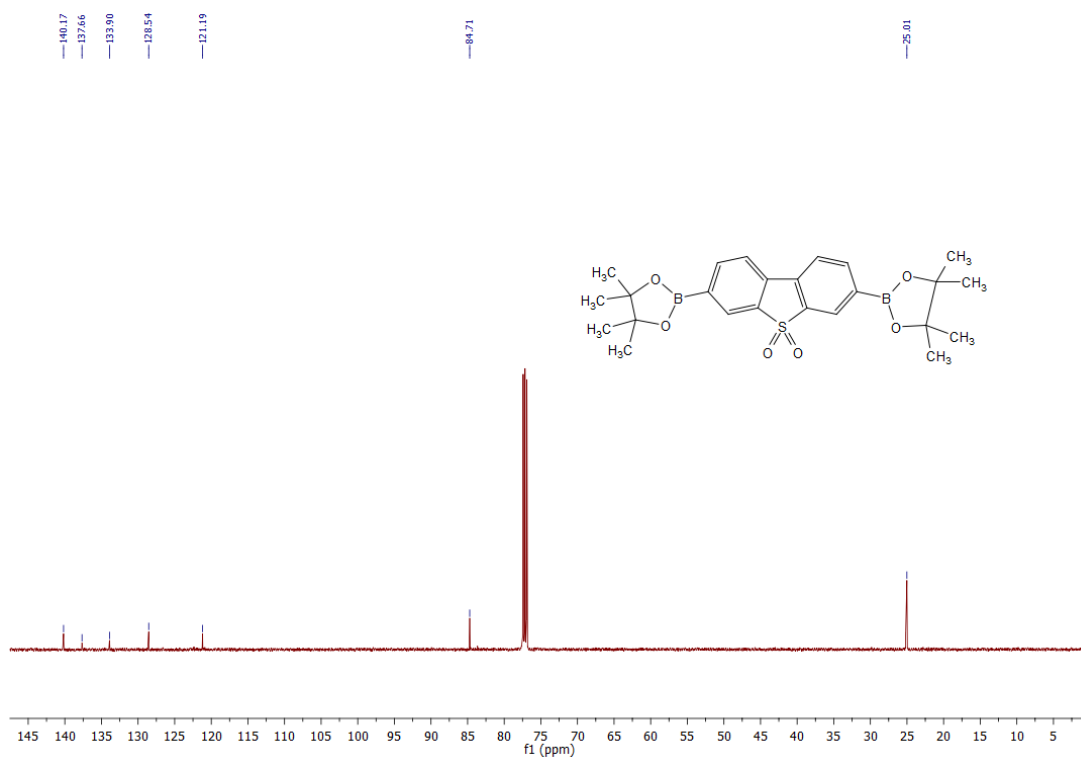


Fig. S40 ¹³C NMR spectrum of 3,7-bis(4,4,5,5-tetramethyl-1,3,2-dioxaborolan-2-yl)dibenzo[b,d]thiophene 5,5-dioxide (**4**) in CDCl₃.

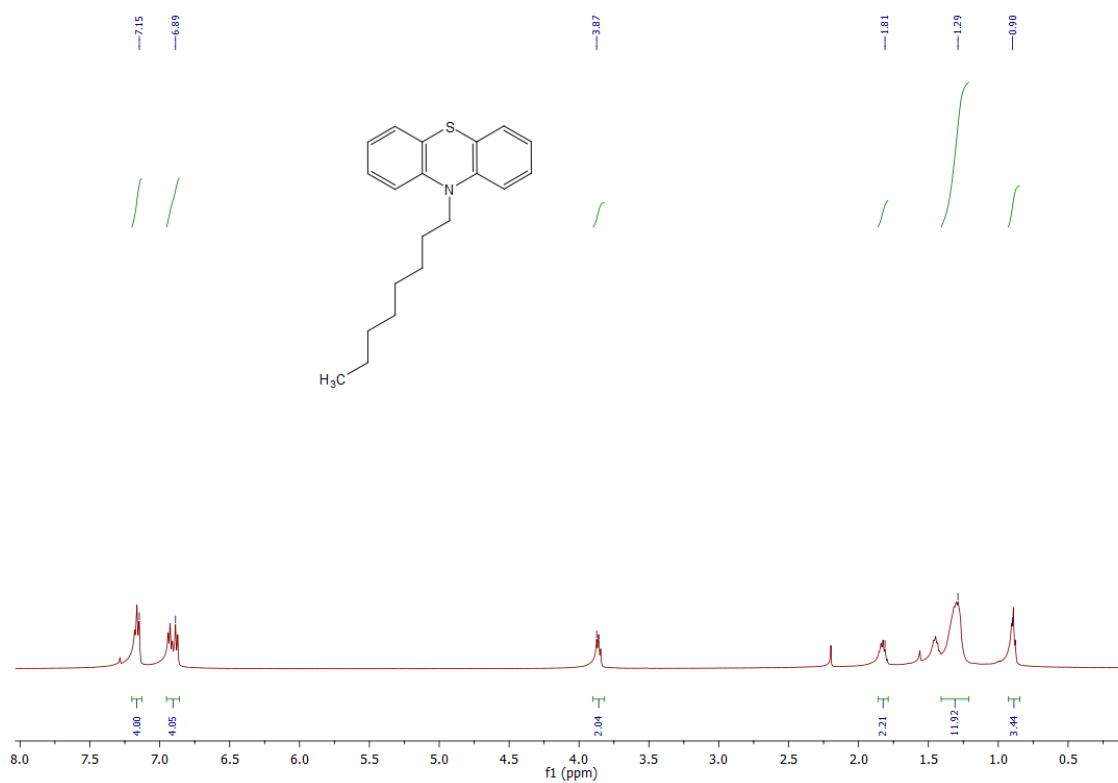


Fig. S41 ^1H NMR spectrum of 10-octyl-10H-phenothiazine (**5**) in CDCl_3 .

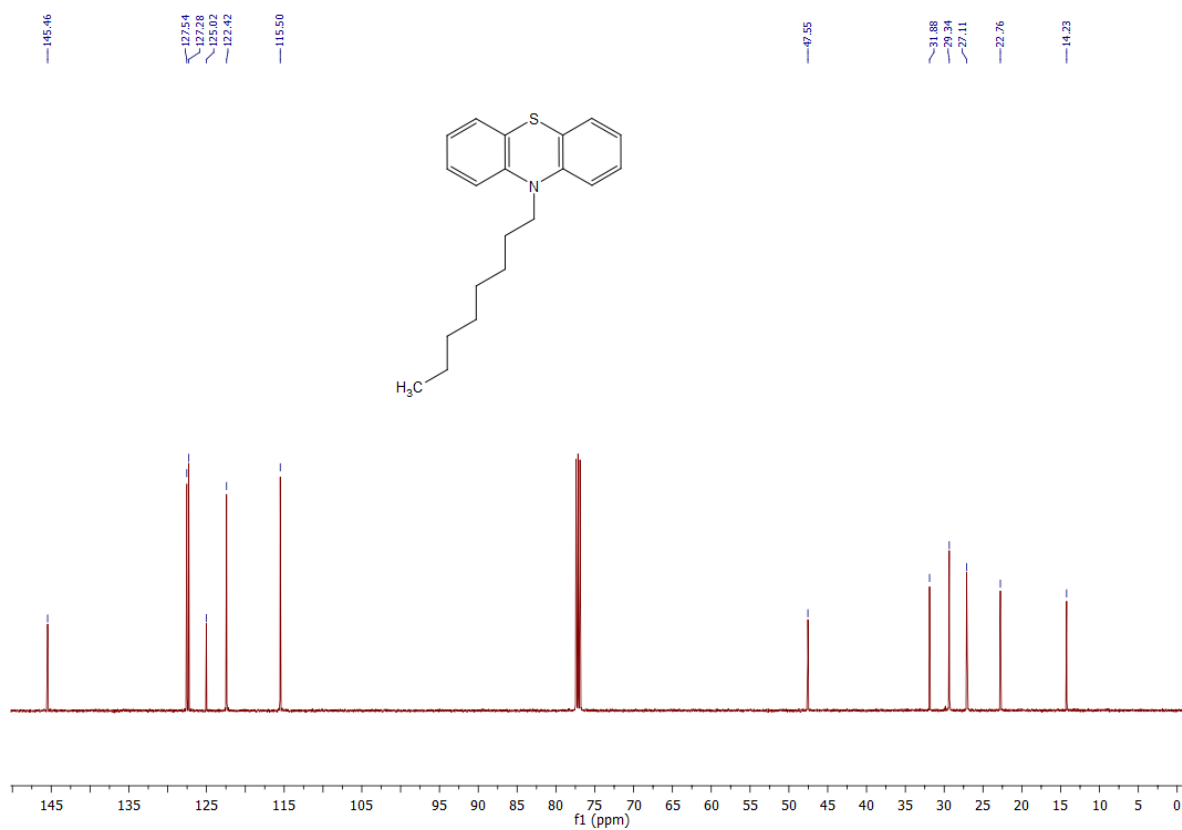


Fig. S42 ^{13}C NMR spectrum of 10-octyl-10H-phenothiazine (**5**) in CDCl_3 .

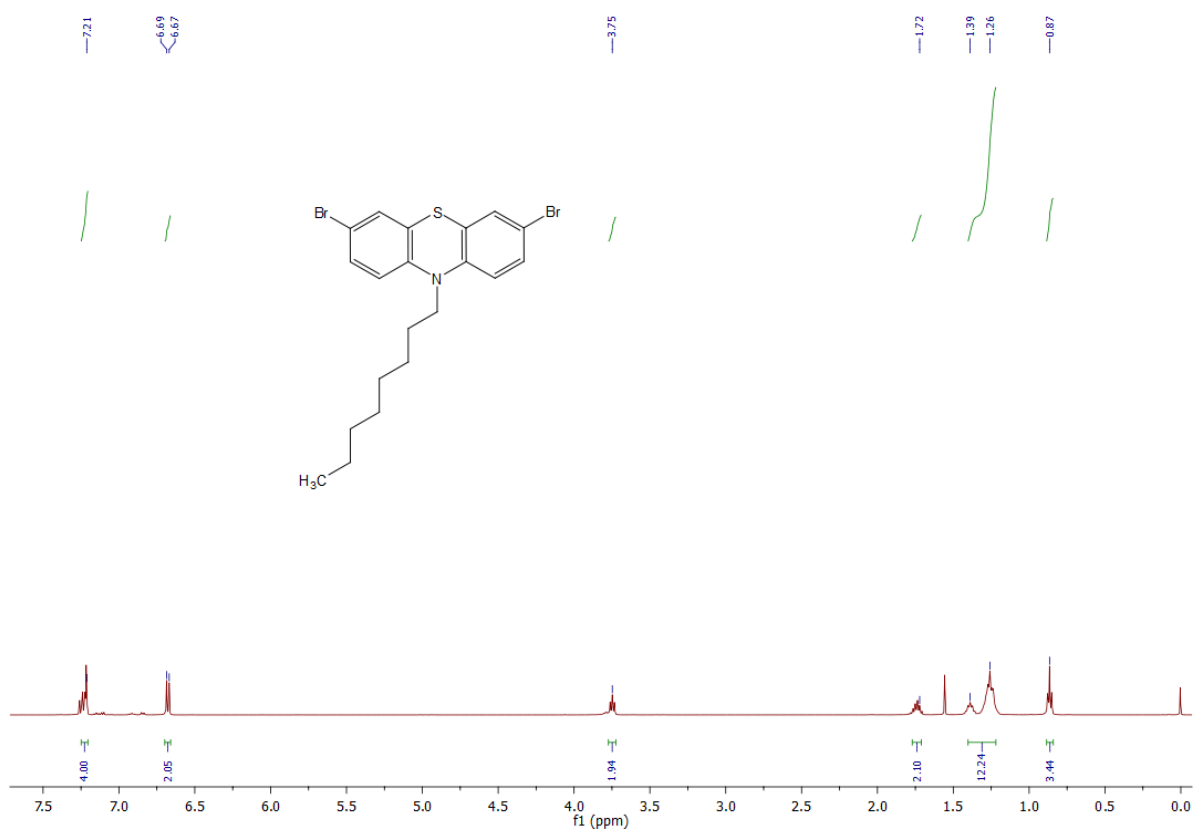


Fig. S43 ¹H NMR spectrum of 3,7-dibromo-10-octyl-10H-phenothiazine (6) in CDCl₃.

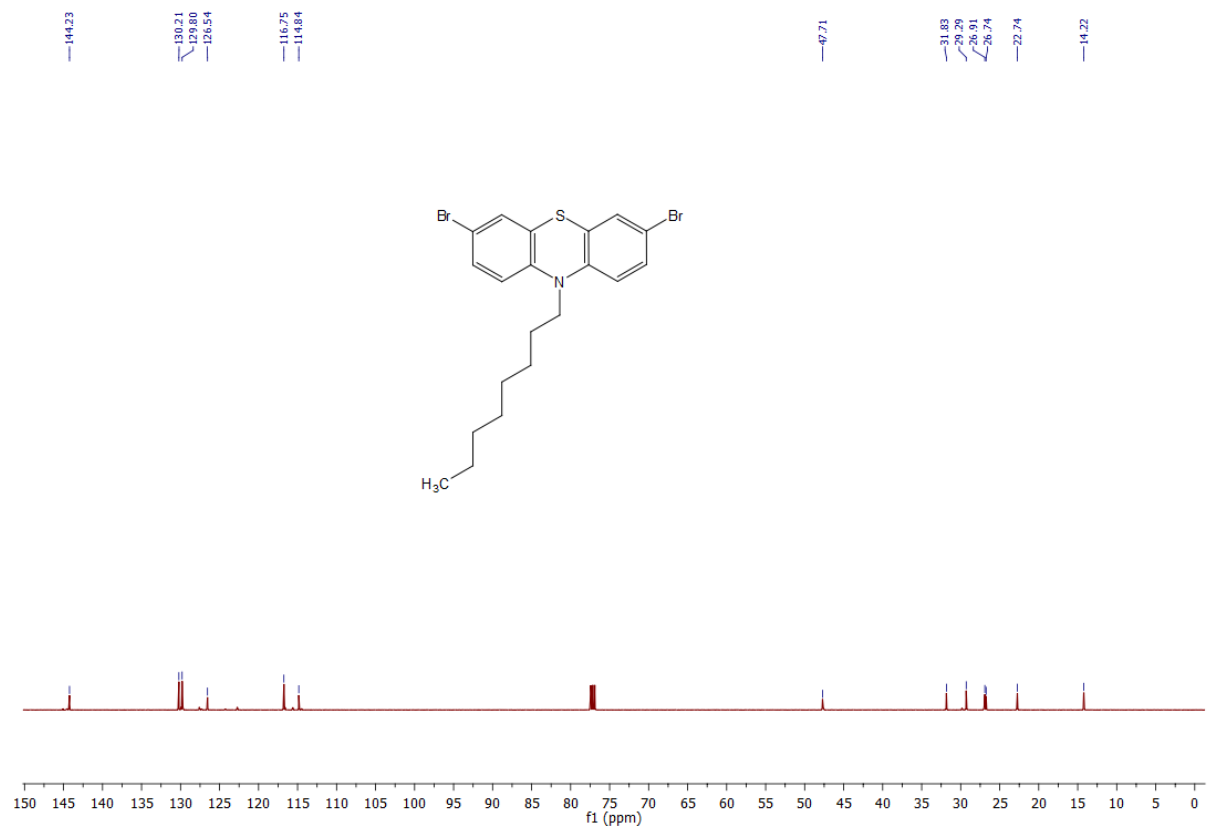


Fig. S44 ¹³C NMR spectrum of 3,7-dibromo-10-octyl-10H-phenothiazine (6) in CDCl₃.

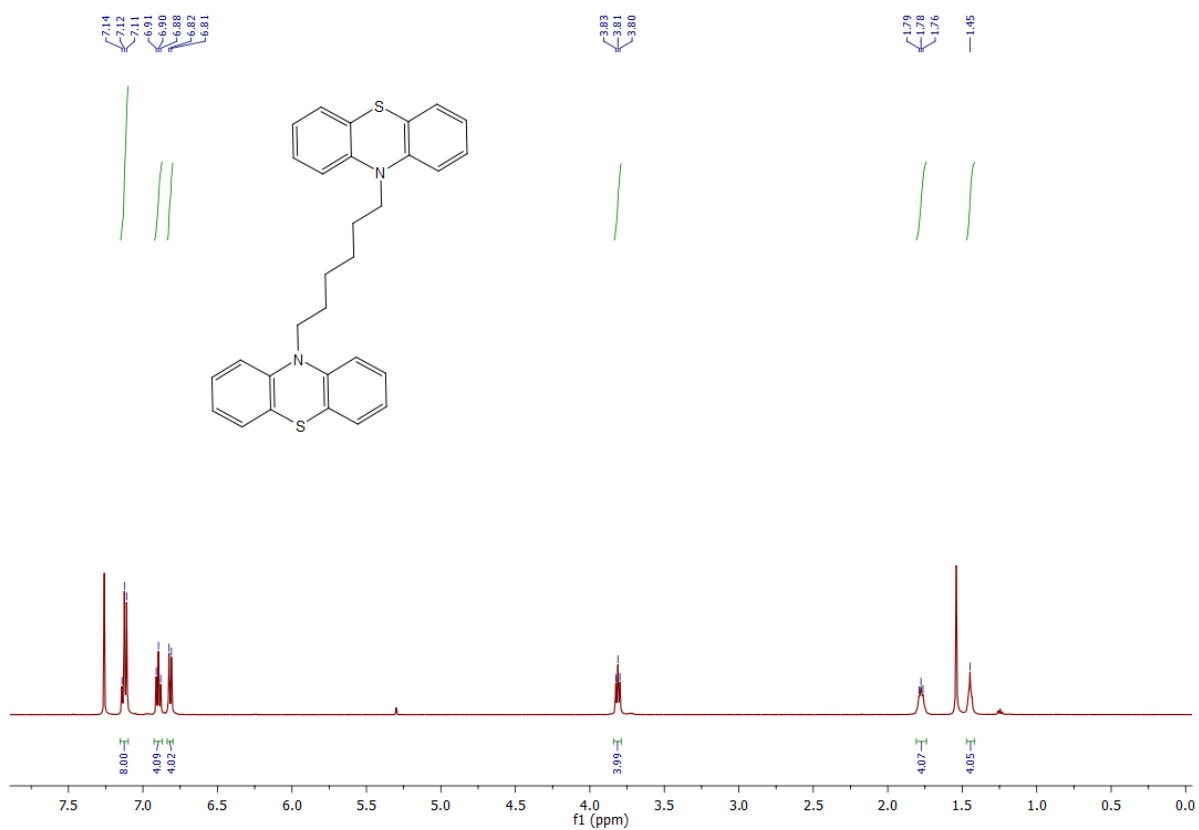


Fig. S45 ^1H NMR spectrum of 1,6-di(10H-phenothiazin-10-yl)hexane (**7**) in CDCl_3 .

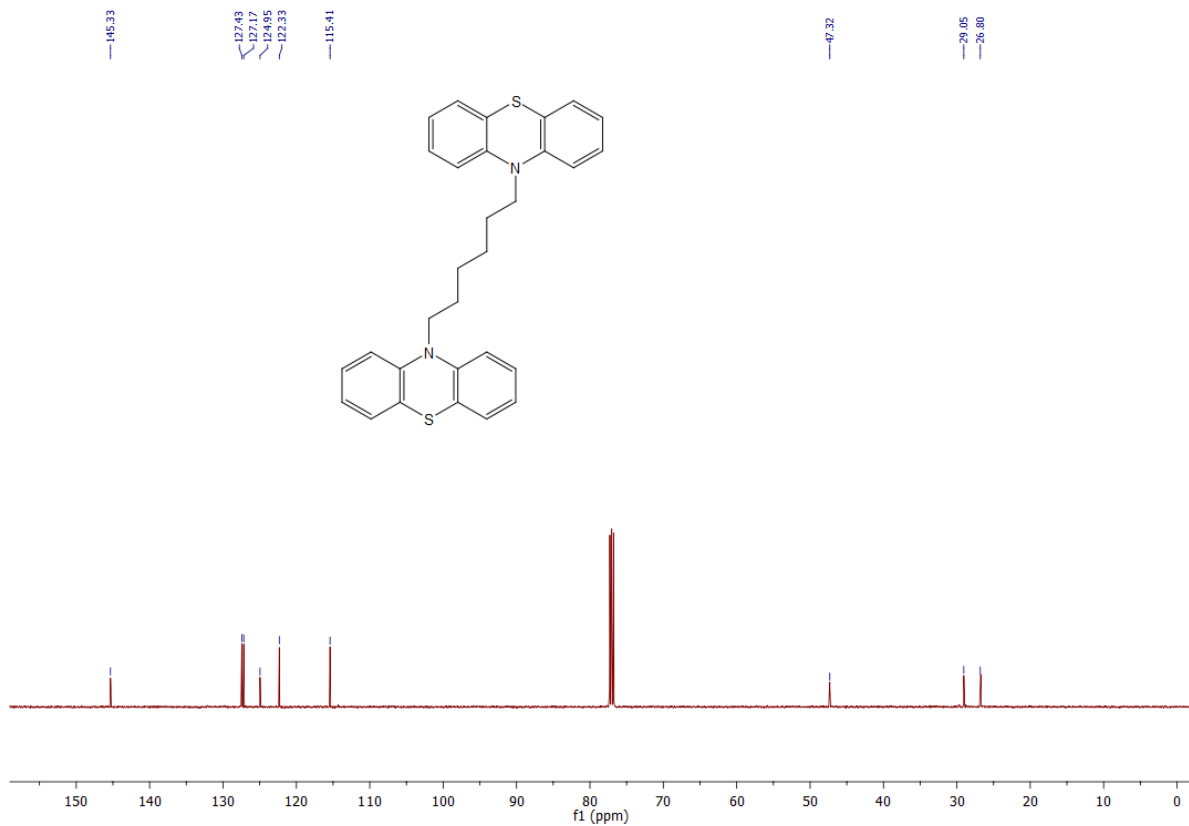


Fig. S46 ^{13}C NMR spectrum of 1,6-di(10H-phenothiazin-10-yl)hexane (**7**) in CDCl_3 .

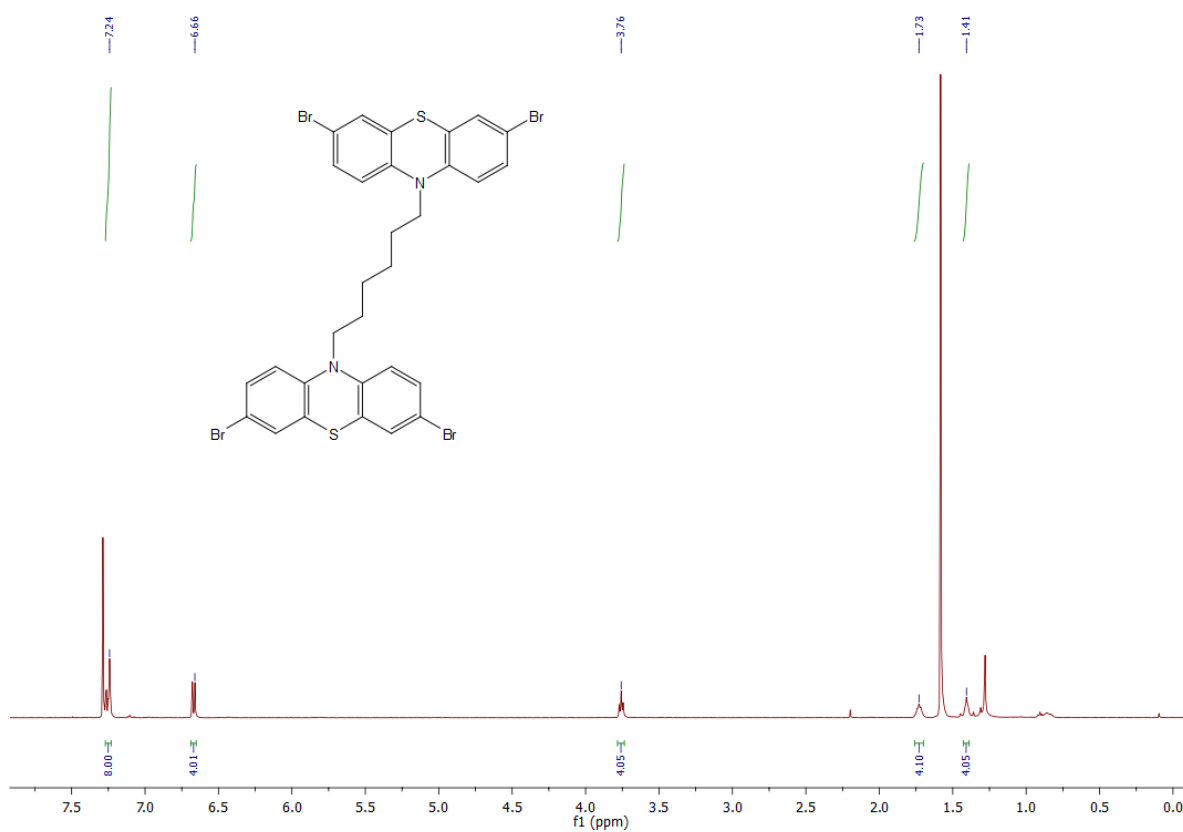


Fig. S47 ¹H NMR spectrum of 1,6-bis(3,7-dibromo-10H-phenothiazin-10-yl)hexane (**8**) in CDCl₃.

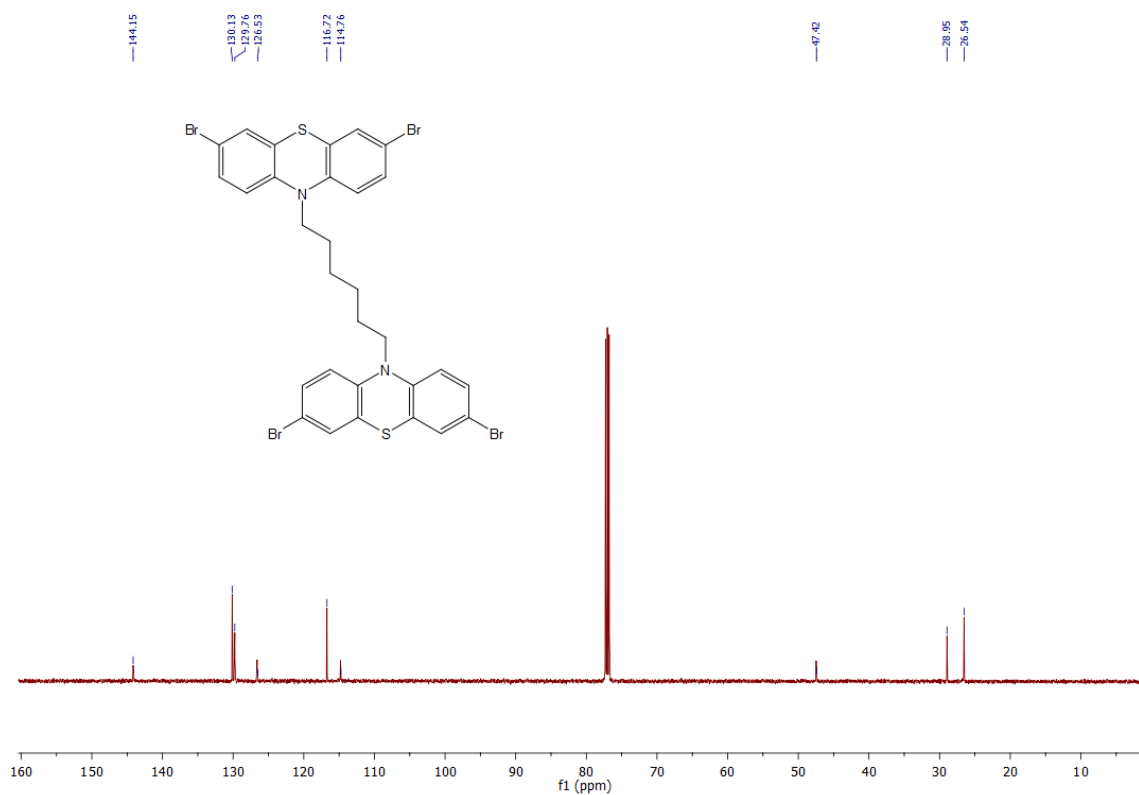


Fig. S48 ¹³C NMR spectrum of 1,6-bis(3,7-dibromo-10H-phenothiazin-10-yl)hexane (**8**) in CDCl₃.

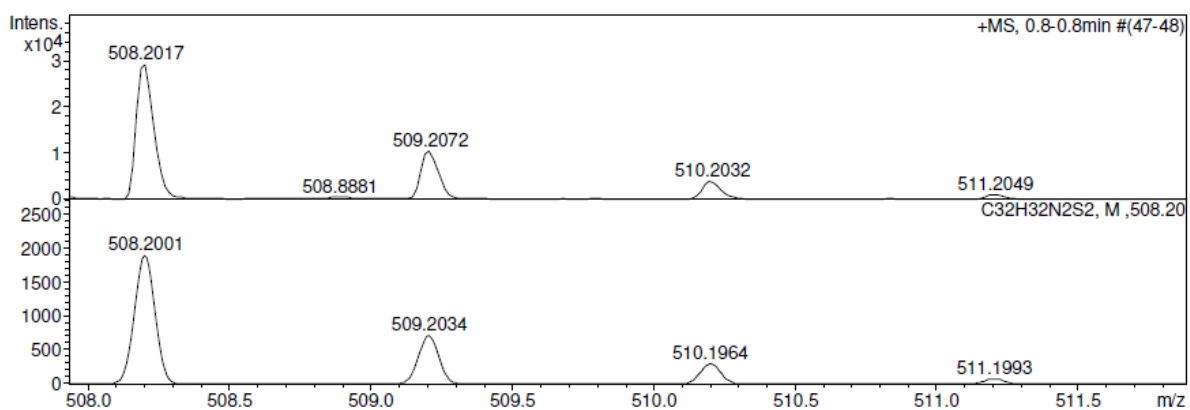


Fig. S49 HRMS (ESI) mass spectrum of 1,8-di(10H-phenothiazin-10-yl)octane (1).

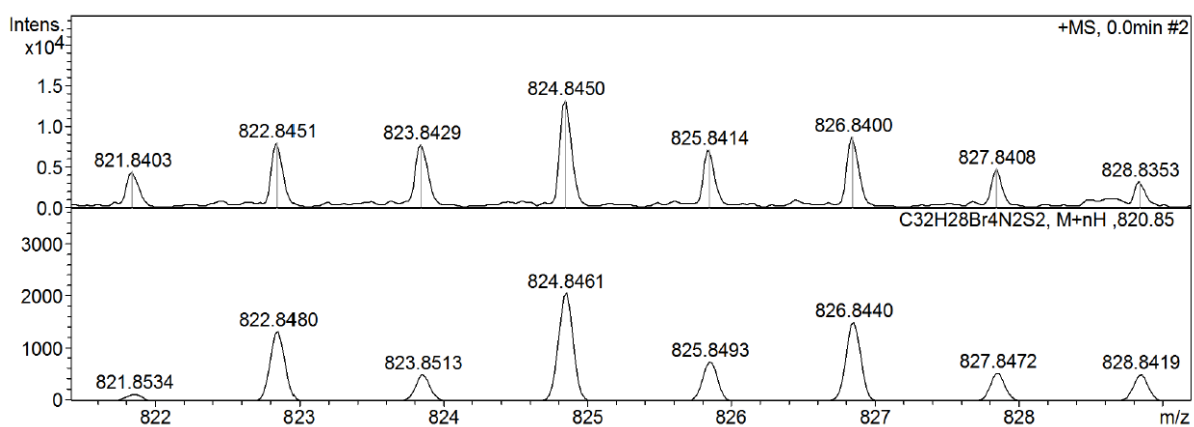


Fig. S50 HRMS (ESI) mass spectrum of 1,8-bis(3,7-dibromo-10H-phenothiazin-10-yl)octane (2).

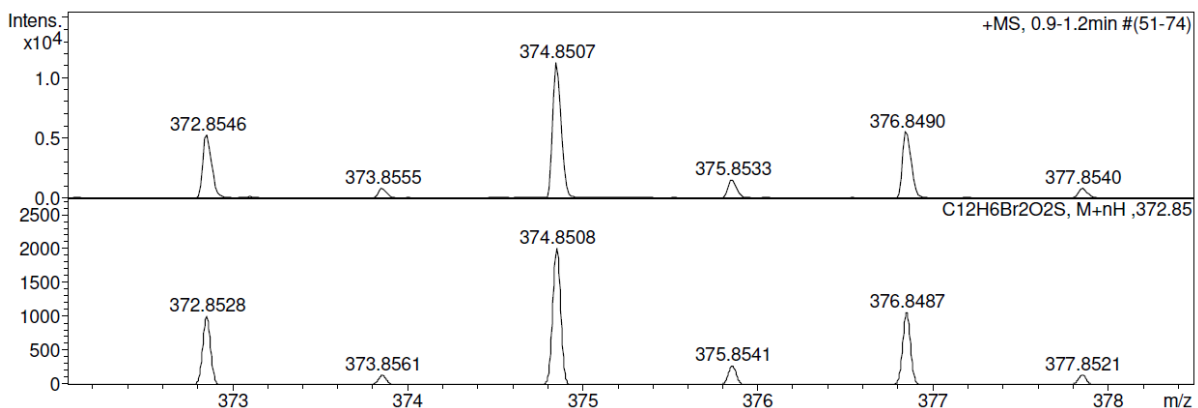


Fig. S51 HRMS (ESI) mass spectrum of 3,7-dibromodibenzo[b,d]thiophene 5,5-dioxide (3).

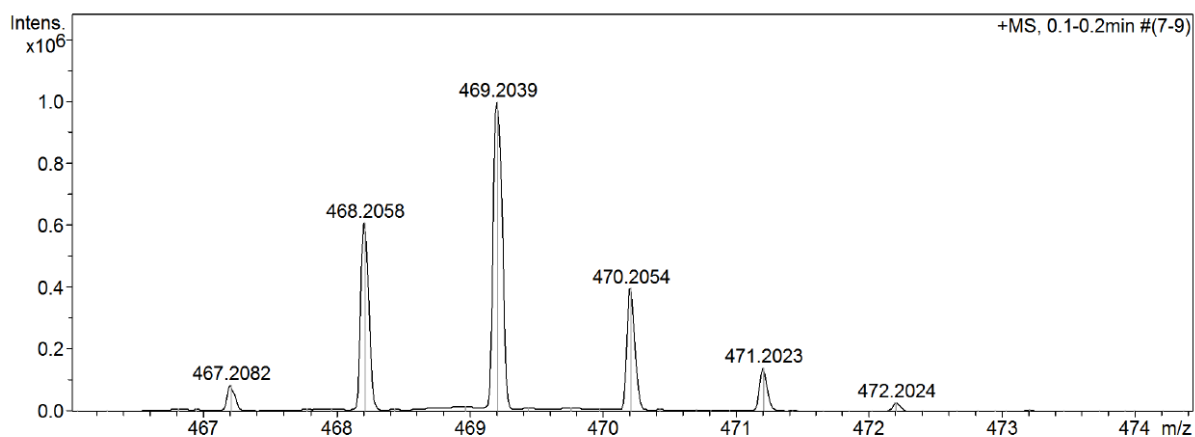


Fig. S52 HRMS (ESI) mass spectrum of 3,7-bis(4,4,5,5-tetramethyl-1,3,2-dioxaborolan-2-yl)dibenzo[b,d]thiophene 5,5-dioxide (**4**).

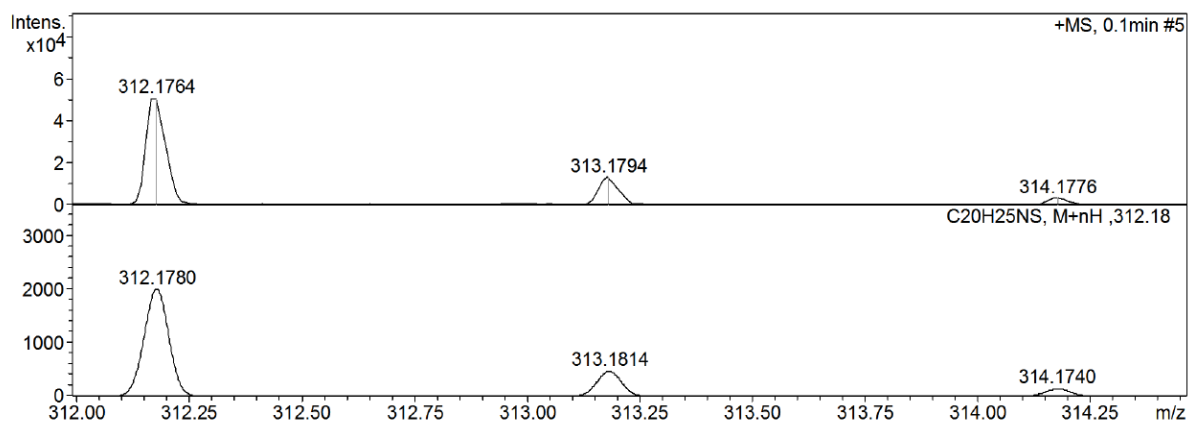


Fig. S53 HRMS (ESI) mass spectrum of 10-octyl-10H-phenothiazine (**5**).

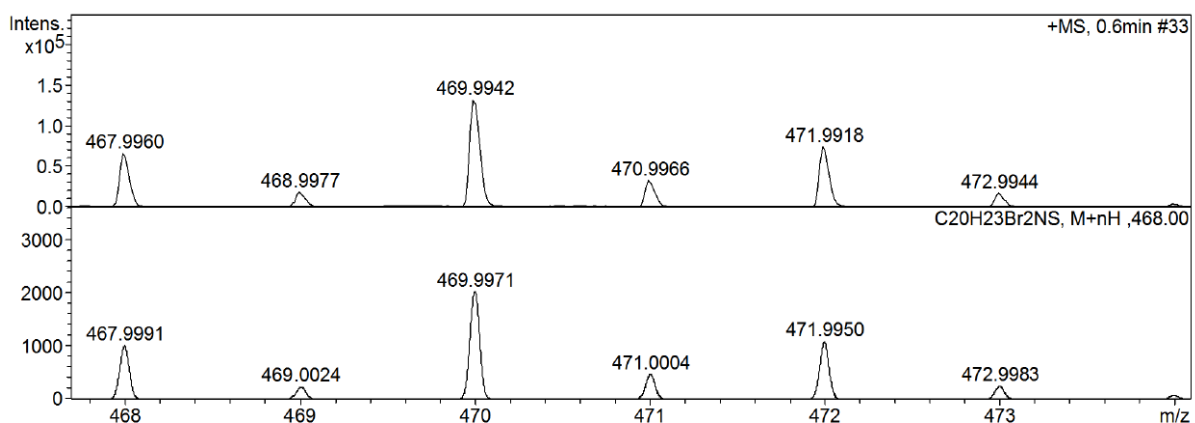


Fig. S54 HRMS (ESI) mass spectrum of 3,7-dibromo-10-octyl-10H-phenothiazine (**6**).

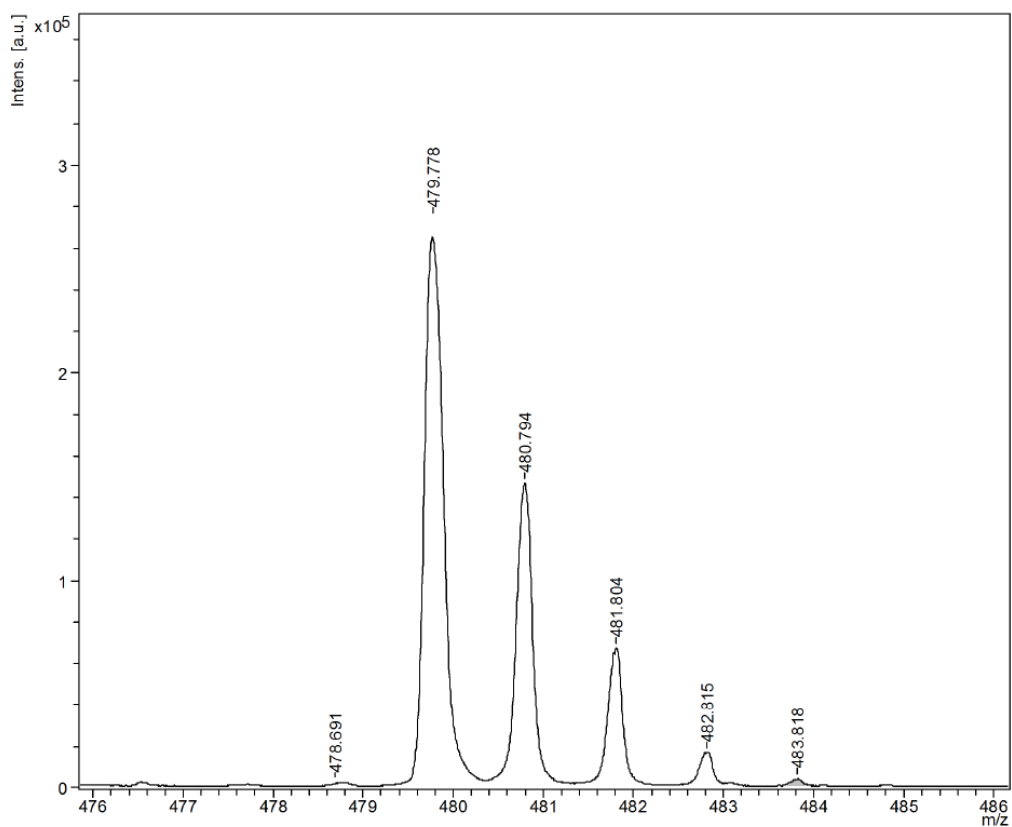


Fig. S55 HRMS (ESI) mass spectrum of 1,6-di(10H-phenothiazin-10-yl)hexane (**7**).

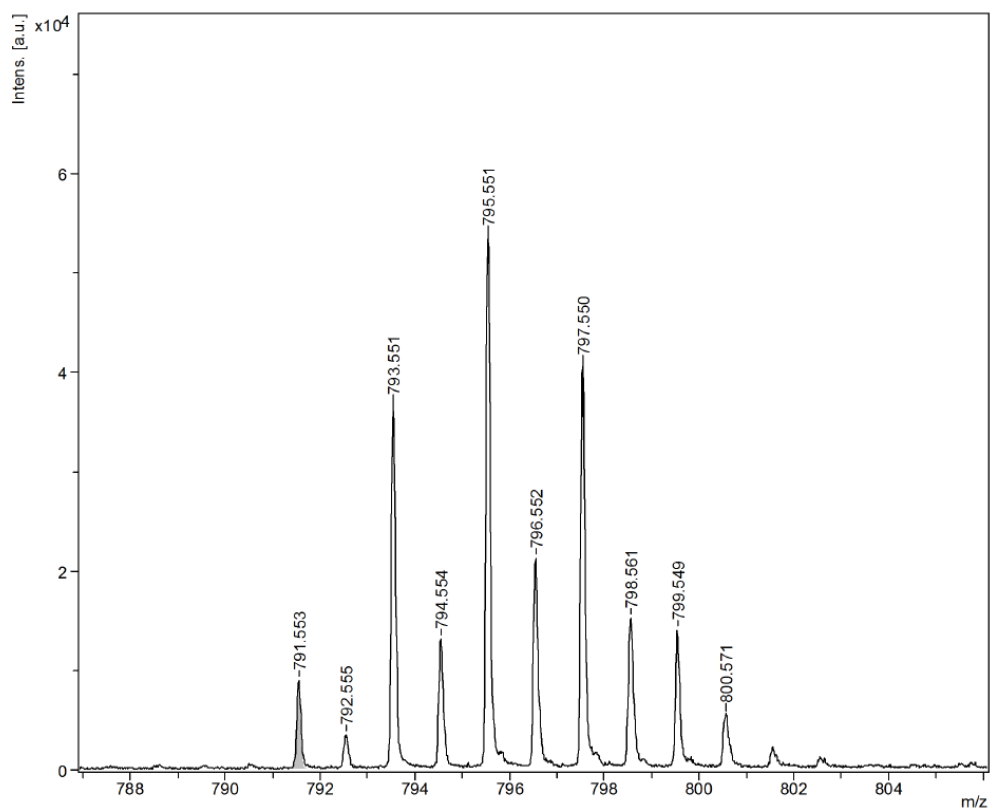


Fig. S56 HRMS (ESI) mass spectrum of 1,6-bis(3,7-dibromo-10H-phenothiazin-10-yl)hexane (**8**).

XVIII. References

1. S. Kundu, B. Behera, A. Giri, N. Saha and A. Patra, *Chem. Commun.*, 2021, **57**, 6875-6878.
2. S. Bandyopadhyay, S. Kundu, A. Giri and A. Patra, *Chem. Commun.*, 2018, **54**, 9123-9126.
3. B. Peterson, D. Ren, L. Shen, Y. Wu, B. Ulgut, G. W. Coates, H. D. Abrun and B. P. Fors, *ACS Appl. Energy Mater.*, 2018, **1**, 3560-3564.
4. S. Xue, Y. Wu, Y. Lu, X. Xu, Q. Sun and W. Yang, *J. Mater. Chem. C*, 2017, **5**, 11700-11707.
5. Z. Wang, X. Yang, T. Yang, Y. Zhao, F. Wang, Y. Chen, J. Zeng, C. Yan, F. Huang and J. Jiang, *ACS Catal.*, 2018, **8**, 8590-8596.
6. A. Laybourn, R. Dawson, R. Clowes, T. Hasell, A. I. Cooper, Y. Z. Khimyak and D. J. Adams, *Polym. Chem.*, 2014, **5**, 6325-6333.
7. B. Sk, S. Khodia and A. Patra, *Chem. Commun.*, 2018, **54**, 1786-1789.
8. Z. Tan, Y. Xing, J. Cheng, G. Zhang, Z. Shen, Y. Zhang, G. Liao, L. Chen and S. Liu, *Chem. Sci.*, 2022, **13**, 1725-1733.
9. Z. Zhang, Y. Wu, K. Tang, C. Chen, J. Ho, J. Su, H. Tian and P. Chou, *J. Am. Chem. Soc.*, 2015, **137**, 8509-8520.
10. H. C. Lim, M. Choi, S. Chae, H. J. Kim, J. Kim and J. Hong, *J. Mater. Chem. C*, 2020, **8**, 11145-11152.
11. V. S. Mothika, P. Sutar, P. Verma, S. Das, S. K. Pati and T. K. Maji, *Chem. - Eur. J.*, 2019, **25**, 3867-3874.
12. J. Pommerehne, H. Vestweber, W. Guss, R. F. Mahrt, H. Bässler, M. Porsch, J. Daub, *Adv. Mater.*, 1995, **7**, 551-554.
13. P. Verma, A. Singh, F. A. Rahimi and T. K. Maji, *J. Mater. Chem. A*, 2021, **9**, 13608-13614.
14. K. Rurack and M. Spieles, *Anal. Chem.*, 2011, **83**, 1232-1242.